Two-proton decay from α-cluster states in ^{10}C and ^{11}N

R. J. Charity,[1] L. G. Sobotka,[1,2] T. B. Webb,[2] and K. W. Brown[1,3]
[1]*Department of Chemistry, Washington University, St. Louis, Missouri 63130, USA*
[2]*Department of Physics, Washington University, St. Louis, Missouri 63130, USA*
[3]*National Superconducting Cyclotron Laboratory, Michigan State University, East Lansing, Michigan 48824, USA*

(Received 14 September 2021; accepted 7 January 2022; published 19 January 2022)

Two-proton decay from excited states in ^{10}C and ^{11}N has been characterized from an analysis of the $2p + 2\alpha$ and $3p + 2\alpha$ exit channels. Data from four previously published invariant-mass studies associated with inelastic excitation, multinucleon knockout, and neutron pickup reactions have been considered. A rotational band in ^{10}C was identified built on the second 0^+ state which has strong α-cluster molecular structure. The members of this band were tentatively identified up to $J^\pi = 4^+$ and all identified states have a prompt $2p$ decay branch. The spins of the 0^+ and 2^+ members were deduced from comparisons of the momentum correlations in their $2p$ branches to those from known $2p$ emitters. The 2^+ and the tentative 4^+ members are both above the α threshold and exhibit large reduced decay widths for α emission. This band exhibits a similar moment of inertia to its analog in the mirror nucleus ^{10}Be. Evidence is also presented for a molecular band in ^{11}N built on the second $3/2^-$ state which $2p$ decays. Tentative members of this band have been assigned up to $J^\pi = 9/2^-$ and their excitation energies also match their likely analogs in the mirror nucleus ^{11}Be.

DOI: 10.1103/PhysRevC.105.014314

I. INTRODUCTION

Ground-state $2p$ emission has been observed in even-Z isotopes beyond the proton drip line. This prompt process is often call "true" $2p$ emission if there is no $(Z-1, A-1)$ intermediate state energetically available for $1p$ decay or democratic if such an intermediate state is available but very wide [1,2]. The latter are typically restricted to light isotopes where the Coulomb barriers to proton emission are small. Both types of $2p$ decay involve similar physics and are treated within the same theoretical frameworks [3–6].

The phenomena of $2p$ emission is not confined to ground states and some of the ground-state $2p$ emitters also have excited states where a rich and complex evolution from prompt to sequential $2p$ decay is observed with increasing excitation energy [7–9]. Moreover, $2p$ emission is not expected to be restricted to the particle-unbound even-Z isotopes. For the odd-Z nuclides both inside and beyond the proton drip line, it is possible that excited states can $2p$ decay. For instance in ^{12}N, the isobaric analog of the $2p$ emitter ^{12}O$_{\text{g.s.}}$ was found to undergo $2p$ decay [10] with the same momentum correlations between the decay products as measured for ^{12}O$_{\text{g.s.}}$ [9]. The isobaric analog state of ^{8}C$_{\text{g.s.}}$ in ^{8}B was also observed to be a $2p$ emitter [11]. The ^{8}C ground state undergoes two sequential steps of $2p$ decay [12,13]. Two-proton decay of the ^{16}Ne$_{\text{g.s.}}$ isobaric analog state in ^{16}F was searched but not found in Ref. [14].

Apart from these analogs of ground-state $2p$ emitters, observations of $2p$ decays of excited states are quite sparse with only the $2p$ decay of two ^{10}C excited states [15] being reasonably well characterized. In this work, we will continue the study of $2p$ decay from ^{10}C excited states and search for $2p$ decay from excited states in its odd-Z neighbor ^{11}N which is located just beyond the proton drip line. Apart from the lowest excited states in these two nuclei, the decay of their states is expected to lead to highly fragmented exit channels, i.e., $2p + 2\alpha$ and $3p + 2\alpha$, respectively. Possible decay paths leading to these channels can be quite varied. These decay paths can include prompt and sequential $2p$ decay as steps in a series of decays leading to the final exit channels. To characterize these, one has to isolate particle-unstable intermediate states produced during these series of decays. Some experience of this has been acquired from the analysis of the $4p + \alpha$ exit channel of ^{8}C [12,13] and the $4p + 2\alpha$ exit channel of ^{12}O [9], but further refinement is needed to isolate weak channels.

Some of the $2p$ emitters observed in this work will be shown to possess strong α-cluster structure. Alpha-clustered states are found in light nuclei typically near the α-emission threshold. The iconic case is the ground state of ^{8}Be that has a shape, as calculated in the *ab initio* Green's function Monte Carlo formalism, which looks like two α particles joined together [16]. This deformed structure is associated with a rotational band with 2^+ and 4^+ members. One can add nucleons to σ and π molecular-like orbits associated with these alpha particles to produce other cluster configurations. Adding a neutron to the π orbital produces the ground state of ^{9}Be which also anchors a rotational band. Molecular bands are also known in ^{9}B, ^{10}Be, and ^{12}Be [17–19]. When the nucleons are added to σ orbits, this tends to push the two α particles apart producing more deformed configurations [17].

In this work we will make use of four data sets using Si and CsI(Tl) detectors from the HiRA apparatus [20] to study the

 ©2022 American Physical Society

states associated with the $2p + 2\alpha$ and $3p + 2\alpha$ exit channels. In the first lowest-energy data set obtain from an experiment at the Texas A&M cyclotron, the $2p + 2\alpha$ channel is produced following the inelastic scattering of an $E/A = 10.7$-MeV ^{10}C beam on 14.1-mg/cm^2 ^{9}Be and 13.4-mg/cm^2 ^{12}C targets. In this experiment, charged particles were detected in an array of four Si-Si E-ΔE telescopes located 14 cm downstream of the target covering polar angles from 5° to 33°. Data from this experiment have previously been published in Refs. [15,21,22] where details of the setup and calibrations can be found. A total of 6×10^4 $2p + 2\alpha$ events were detected.

Three higher-energy data sets are included all utilizing almost identical HiRA setups in experiments perform at the National Superconducting Cyclotron Laboratory at Michigan State University. These include a mixed ^{15}O (≈89%, $E/A =$ 48.1 MeV) plus ^{17}Ne (≈11%, $E/A = 58.2$ MeV) secondary beam [8,14,23–25], an ^{13}O secondary beam of $E/A = 65.4$ MeV [9,26–29] and an $E/A = 67$-MeV ^{9}C secondary beam [11–13,24]. These secondary beams were incident on a 1-mm-thick ^{9}Be target and charged particles were detected in 14 Si-CsI(Tl) E-ΔE telescopes located 80 cm downstream of the target covering polar angle from 2.1° to 12.4°. With the $A > 10$ secondary beams, excited states in ^{11}N and ^{10}C were produced via multinucleon knockout reactions either directly or indirectly following sequential charged-particle emission. Only the ^{13}O data set populated the $3p + 2\alpha$ exit channel with significant yield (3×10^5 events). For the ^{9}C secondary beam, ^{10}C states were populated via neutron pickup reactions and only 1.2×10^4 $2p + 2\alpha$ events were detected. The ^{13}O data set has the highest $2p + 2\alpha$ statistics with 2×10^6 events followed by the ^{15}O / ^{17}Ne data set with 8×10^5 events.

II. ^{10}C STATES DECAYING TO THE $2p + 2\alpha$ EXIT CHANNEL

The $2p + 2\alpha$ exit channel can have contributions from ^{10}C states that decay by many different decay paths. For example, α and proton decays lead to ^{6}Be and ^{9}B states which are both particle unstable, even in their ground states, and their decay leads to this final exit channel. In addition, two-proton decay leads to ^{8}Be states which breakup into two α particles again producing the $2p + 2\alpha$ channel. By selecting events associated with different intermediate states, we are better able to separate states which decay via these different paths. This selection on intermediate states helps isolate levels produced with low intensity. In general, it is quite difficult to select out a particular intermediate state. For example, one could attempt to find events associated with a ^{6}Be$_{\text{g.s.}}$ intermediate state which has a small decay width of 96 keV by looking at the invariant mass of the $p + 2\alpha$ subevents. As all $2p + 2\alpha$ events produce two different $p + 2\alpha$ subevents, then even if all events are associated with one ^{6}Be$_{\text{g.s.}}$ intermediate state, the $p + 2\alpha$ invariant-mass spectrum will still have a significant background under the ^{6}Be$_{\text{g.s.}}$ peak. Attempts to subtract this background by gating on a neighboring region of the $2p + \alpha$ spectra next to the ^{6}Be$_{\text{g.s.}}$ peak are frustrated by the fact that a single event can contribute to both the ^{6}Be$_{\text{g.s.}}$ peak and to this background region from its different subevents.

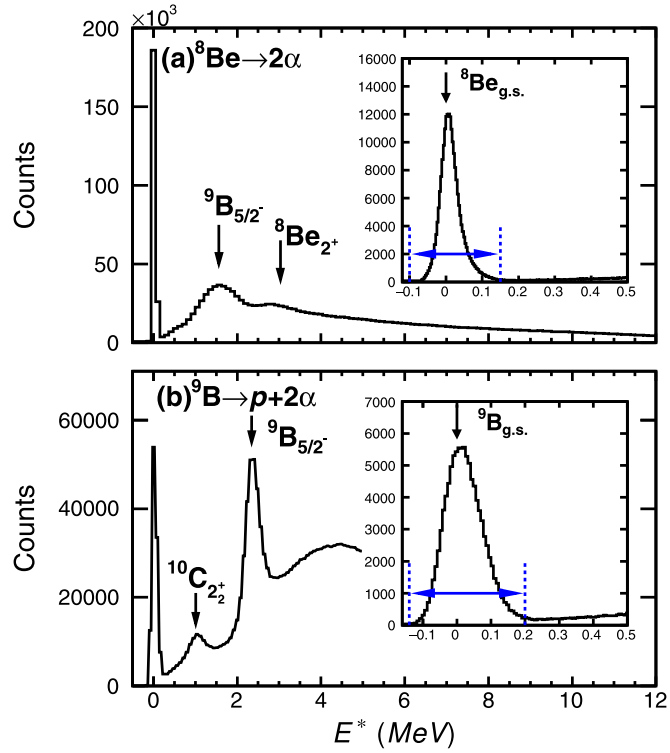

FIG. 1. Distributions of ^{8}Be and ^{9}B excitation energy E^* for (a) 2α and (b) $p + 2\alpha$ subevents in the detected $2p + 2\alpha$ events from the ^{13}O data set. The insets in both panels show an expanded view of the ^{8}Be and ^{9}B ground-state peaks where the bin size on the energy axis is decreased. The sources of the observed peaks are indicated. The figure also demonstrates that correlations from decay of states can be visible in the invariant-mass distributions of the subevents. For example the peak at ≈1 MeV in panel (b) is produced by the decay of the second 2_2^+ state of ^{10}C. This state proton decays to the ground state of ^{9}B. This peak is produced by the subevent comprised of the first-emitted proton and the α particles produced in the decay of ^{9}B. Similarly, the $5/2^-$ state in ^{9}B produces a broad peak in the invariant mass of the 2α subevents in panel (a).

However, there are two intermediate states which can be gated on very cleanly, namely, ^{8}Be$_{g.s}$ and ^{9}B$_{\text{g.s.}}$ because they are very narrow and located just above threshold where background contributions to the invariant mass from all sources are typically negligible. Figure 1 shows the excitation-energy spectra of the 2α and $p + 2\alpha$ subevents where the resonance peaks associated with these ground states are very prominent. The regions around the ground-state peaks has been expanded in the insets showing that the background under these peaks is small and the gates utilized in the subsequent analysis are displayed. As ^{9}B$_{\text{g.s.}}$ decays sequentially through ^{8}Be$_{\text{g.s.}}$, these gates can be used to subdivide all events into three groups: (a) those that decay though ^{9}B$_{\text{g.s.}}$ and hence also through ^{8}Be$_{\text{g.s.}}$, (b) those that decay through ^{8}Be$_{\text{g.s.}}$ but not through ^{9}B$_{\text{g.s.}}$, and (c) those that do not decay through ^{8}Be$_{\text{g.s.}}$.

Invariant-mass distributions for these three subdivisions of the events for each of the ^{13}O, ^{10}C, and ^{15}O / ^{17}Ne data sets are shown in Fig. 2. Peaks identified in these spectra are labeled by letters and the spins and parities we assigned

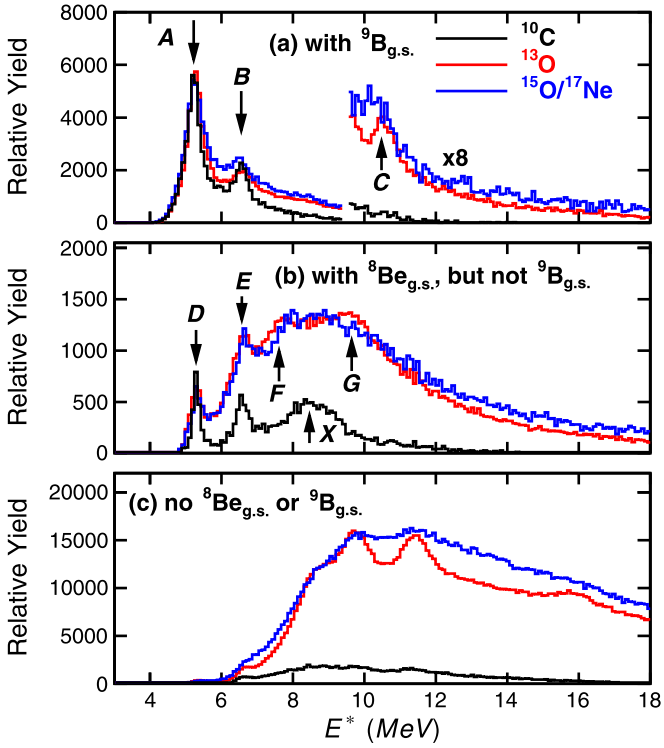

FIG. 2. Distributions of ^{10}C excitation energy obtained from $2p + 2\alpha$ events, with the invariant-mass method, from three of the data sets studied in this work. Panel (a) is for events which decayed through a $^{9}B_{g.s.}$ intermediate state, panel (b) is for events which decayed through an $^{8}Be_{g.s.}$ intermediate state but not a $^{9}B_{g.s.}$ state, and panel (c) is for the remaining events. Peaks discussed in this work are labeled by letters. The results from each data set have been normalized so that the 2_2^+ peaks in panel (a) have the same maximum value.

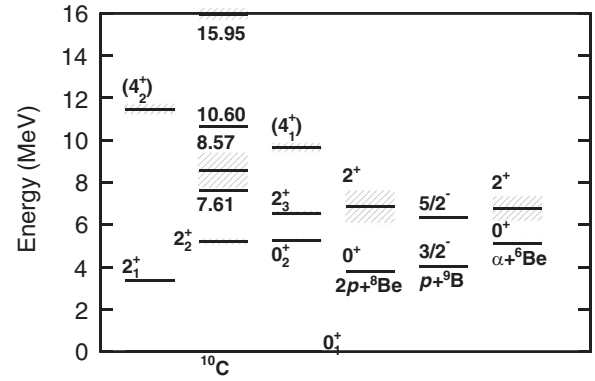

FIG. 3. Level scheme for ^{10}C showing the levels discussed in this work and their energies relative to the intermediate states. The levels are labeled by their spin, or if that is unknown, by their excitation energy in MeV.

to them (Secs. IV and V) are listed in Table I. A ^{10}C level scheme from this work is shown in Fig. 3, where, for comparison, the energies of the intermediate states are also shown.

For the events decaying through a $^{9}B_{g.s.}$ intermediate state [Fig. 2(a)], the invariant-mass spectra are all dominated by peak *A* at 5.222 MeV associated with the 2_2^+ excited state [30]. We have normalized the spectra from each data set to give a similar yield for this peak. Peak *B* is also present in each of the three data sets. Finally, the ^{13}O and ^{15}O / ^{17}Ne data sets show evidence of a higher-energy peak (*C*) at 10.6 MeV. Possibly this is the same as the 10.48-MeV peak identified in the proton pickup reaction with a ^{9}C beam [13], but where the decay path was not determined.

TABLE I. Level parameters obtained from the fits to the $2p + 2\alpha$ invariant-mass spectra of Figs. 4 and 6. A number of peaks observed in different exit channels at the same energy have been treated as decay branches of common parent states. The extracted branching ratios (BR) are listed but, except for the 2_3^+ state, these have not been corrected for detector efficiency. Spin assignments, when made, are also listed. The uncertainties listed are statistical, in addition there is a systematic uncertainty of 10 keV in the centroids [9,24].

J^{π}	E^{*} [MeV]	Γ [keV]	Peak	Branch	BR	Data sets
2_2^+	5.222(4)	250(46)	*A*	$p + {}^{9}B_{g.s.}$		^{10}C, ^{13}O, ^{15}O / ^{17}Ne
0_2^+	5.282(5)	96(57)	*D*	$2p + {}^{8}Be_{g.s.}$	$> 30\%$	^{10}C, ^{13}O, ^{15}O / ^{17}Ne
2_3^+	6.556(10)	177(75)	*B*	$p + {}^{9}B_{g.s.}$	66(2)%	^{10}C, ^{13}O, ^{15}O / ^{17}Ne
			E	$2p + {}^{8}Be_{g.s.}$	18(1)%	
			H	$\alpha + {}^{6}Be_{g.s.}$	16(1) %	
	7.61(9)	< 450	*F*	$2p + {}^{8}Be_{g.s.}$		^{13}O
$1^+, 2^{\pm}, 3^{\pm}, 4^+$	8.57(2)	1645(40)	*L*	$p + {}^{9}B_{5/2^-}$		^{13}O, ^{15}O / ^{17}Ne, ^{10}C(?)
(4_1^+)	9.647(21)	392(90)	*N*	other	46(2)%[a]	^{9}C, ^{13}O, ^{15}O / ^{17}Ne
			I	$\alpha + {}^{6}Be_{g.s.}$	27(2)%[a]	
			M	$p + {}^{9}B_{5/2^-}$	23(1)%[a]	
			G	$2p + {}^{8}Be_{g.s.}$	3.6(6)%[a]	
	10.603(23)	< 230	*C*	$p + {}^{9}B_{g.s.}$		^{13}O, ^{15}O / ^{17}Ne
(4_2^+)	11.450(9)	481(56)	*O*	other	86(1)%[a]	^{9}C, ^{13}O, ^{15}O / ^{17}Ne
			J	$\alpha + {}^{6}Be_{g.s.}$	9(1)%[a]	
				$p + {}^{9}B_{5/2^-}$	4.1(4)%[a]	
	15.953(24)	551(116)	*P*	other	88(2)%[a]	^{13}O
			K	$\alpha + {}^{6}Be_{g.s.}$	12(2)%[a]	

[a]Branching ratios are not corrected for channel-dependent detector efficiencies.

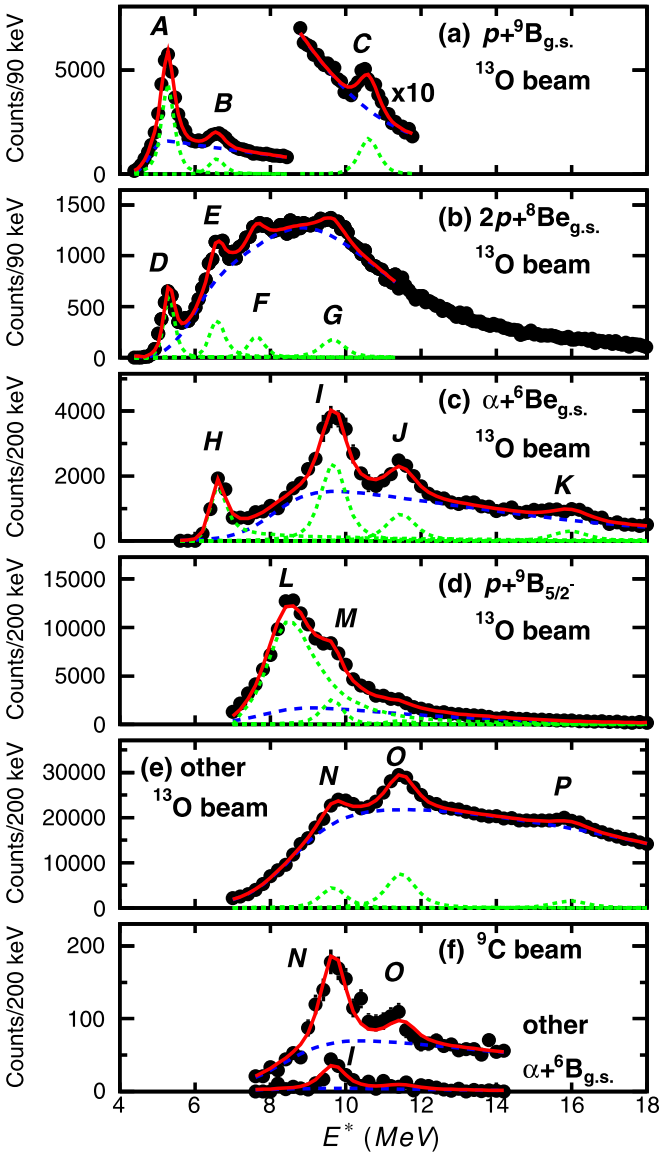

FIG. 4. (a)–(e) Distributions of ^{10}C excitation energy extracted from the ^{13}O data set for the specified decay paths. (f) Distributions obtained with the ^{9}C data set. The solid-red curves show fits to these distributions with the dashed-blue curves showing the fitted background contributions and the dotted-green curves indicating the contribution from each of the resonances. Labels for the observed peaks are given.

Figure 2(b) shows the invariant-mass distributions for events which decay through an ^{8}Be$_{g.s.}$ intermediate state, but are not fed by the decay of ^{9}B$_{g.s.}$. Peaks D and E are prominent in the spectra from all three data sets and are associated with prompt $2p$ decays. The lower of these two peaks is identified as the $J^{\pi} = 0_2^+$ state and is discussed in Sec. IV A. Peak X in the ^{10}C data set is not associated with a ^{10}C excited state and was attributed to target contamination in Ref. [15]. Also of interest are two other less prominent peaks, F and G, which are only observed in the ^{13}O data set and are best seen in Fig. 4(b), where the spectrum from this data set is shown by itself.

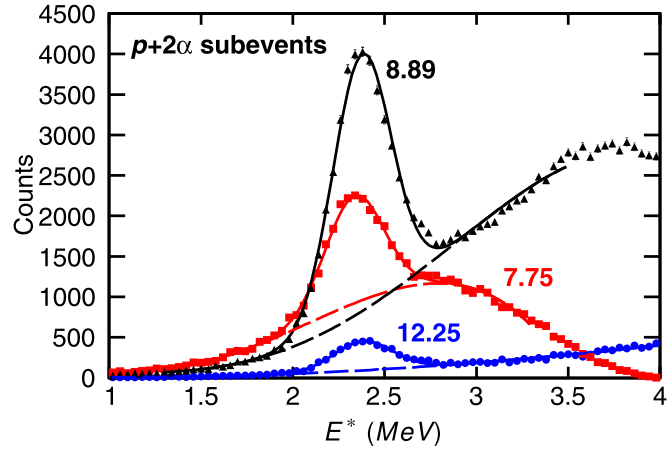

FIG. 5. Distributions of ^{9}B excitation energy from the invariant mass of $p + 2\alpha$ subevents obtained from $2p + 2\alpha$ events with no ^{8}Be$_{g.s.}$ intermediate fragments and with a 500-keV-wide gate on the ^{10}C excitation energy. The results here are from the ^{13}O data set and the distributions are labeled by the mean ^{10}C excitation energy of the gate. The solid curves are from fits with Gaussian peaks at the energy for the $5/2^-$ state in ^{9}B plus smooth polynomial backgrounds (dashed curves).

The third category of events, those that do not decay through an ^{8}Be$_{g.s.}$ intermediate state [Fig. 2(c)], show evidence of additional peaks which are most pronounced in the ^{13}O data set. This category of events contains a number of possibilities, including α decay to ^{6}Be$_{g.s.}$ ($\Gamma = 92$ keV), proton decay to the $5/2^-$ ($E^* = 2.345$ MeV, $\Gamma = 81$ keV) state of ^{9}B [which has a negligible branching ratio (0.5%) through ^{8}B$_{g.s.}$], and decay paths involving much wider intermediate states. Contribution from wider intermediate states are very difficult to isolate, but the first two possibilities can be explored with an alternative gating scheme which, while it cannot separate these decays on an event-by-event basis, can give their excitation spectra.

In this scheme, the third category of events are subdivided into bins of ^{10}C excitation energy and the ^{9}B and ^{6}Be excitation-energy distributions from the invariant-mass of $p + 2\alpha$ and $2p + \alpha$ subevents are constructed. For example, Fig. 5 shows the ^{9}B excitation-energy distributions from three 500-keV-wide gates on the ^{10}C excitation energy centered at 7.75, 8.89, and 12.75 MeV. The $5/2^-$ state of ^{9}B at $E^* = 2.345$ MeV is clearly visible in all spectra where its width is dominated by the experimental resolution. Such distributions are fit (solid curves) with a Gaussian peak plus a smooth polynomial background (dashed curves). The integrated peak values are then used to construct, point-by-point, the ^{10}C excitation spectra consistent with decays through ^{6}Be$_{g.s.}$ and ^{9}B$_{5/2^-}$. With the high-statistics ^{13}O data set, this procedure was performed with narrow 200-keV-wide gates of the ^{10}C excitation energy. The resulting spectra are shown Figs. 4(c) and 4(d) where a number of peaks are visible. After removing these last two contributions, the residual excitation spectrum for which no decay path has been determined is shown in Fig. 4(e) and it too displays a number of peaks.

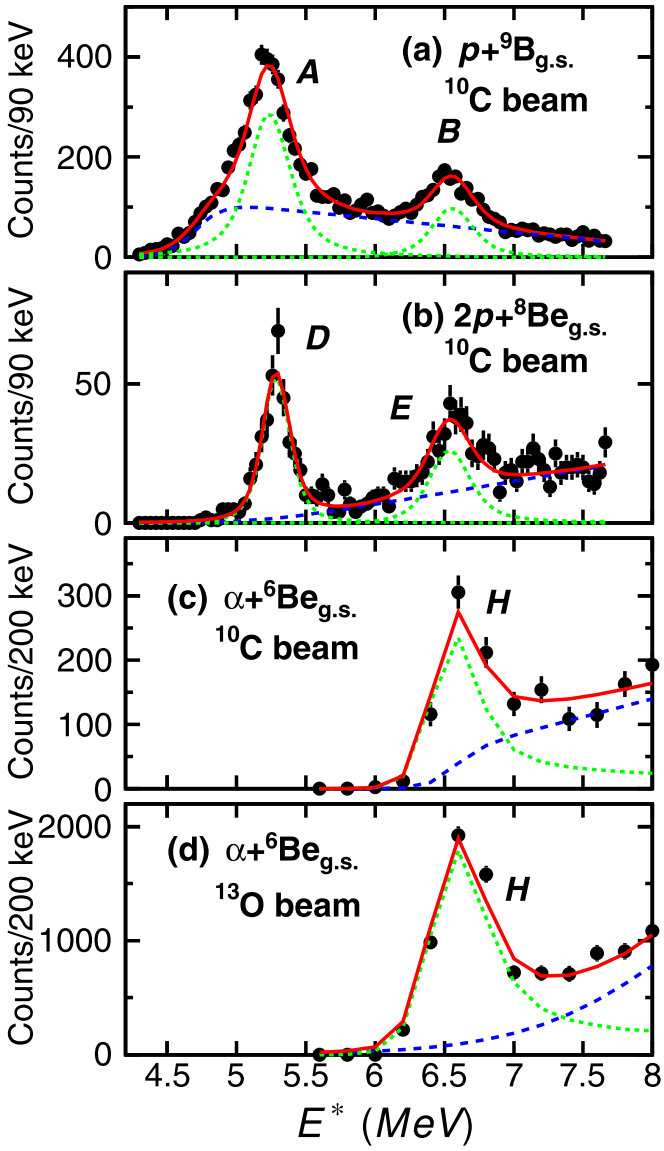

FIG. 6. (a)–(c) Distributions of ^{10}C excitation energy extracted from the ^{10}C data set for the specified decay paths. The lower-statistics $\alpha + {}^6\mathrm{Be}_{g.s.}$ distribution in panel (c) is compared with the higher-statistics version from the ^{13}O data set in panel (d). The solid-red curves show fits to these distributions with the dashed-blue curves showing the fitted background contributions and the dotted-green curves indicating the contribution from each of the resonances. Labels for each of the observed peaks are given. The fitted curves have the same binning in E^* as the experimental data.

Fits to invariant-mass spectra are shown in Figs. 4 and 6 as the solid red curves. These fits, and others presented in this work, include smooth background contributions (dashed-blue curves) associated with nonresonant contributions and wide unresolved resonances. As these backgrounds contributions cannot be presently calculated, our assumption is they represent the smooth behavior under the visible peaks. We fit the background using an inverse-Fermi function times a polynomial. The inverse Fermi function allows the fitted background to vanish as one decreases the decay energy towards the channel threshold. The polynomial is generally taken to be of first or second order. For narrow peaks sitting on small backgrounds, the choice of the background parametrization has little effect on the extracted peak parameters. The choice of background parametrization will be more important for wider peaks. For the very wide peaks the differentiation between peak and background is not possible and the peak becomes part of the background.

For the resolved resonances in these figures we have assumed Breit-Wigner intrinsic lineshapes with the experimental resolution and efficiency included via Monte Carlo simulations [24] except for a few cases where R-matrix intrinsic lineshapes are utilized instead. The energy resolution of the detectors in the simulations have been fine tuned so as to reproduce the experimental lineshapes of the $^8\mathrm{Be}_{g.s.}$, $^9\mathrm{B}_{g.s.}$, $^9\mathrm{B}_{5/2^-}$, and $^6\mathrm{Be}_{g.s.}$ intermediate states observed in the invariant-mass spectra of the subevents (Fig. 1). At $E^* = 6.54$ MeV, the FWHM of the simulated ^{10}C resolution is 252(38) keV and 340(20) keV for the low-energy ^{10}C inelastic scattering and higher-energy data sets, respectively.

The centroids and widths of the low-energy resonances have been largely determined from fits to the ^{10}C inelastic-scattering data set due to its superior energy resolution and peak-to-background ratios. Figure 6 shows such fits to peaks A, B, D, E, and H. Peaks B, E, and H has been assumed to be decay branches of the same state and so a single centroid and width were obtained from a joint fit to all the spectra in this figure. Originally we tried fitting these peaks with Breit-Wigner lineshapes, but found some tension in fitting the width of peak B and the low-energy tail of peak H at the same time. This was resolved by using R-matrix lineshapes associated with the spin assignment of 2^+ (see Sec. IV D). The α-decay branch has the highest threshold and with an $\ell = 2$ centrifugal barrier, the barrier penetration factor rises rapidly in the vicinity of the peak giving this decay branch a skewed lineshape. This allowed a better joint fit to the spectra and to the $\alpha + {}^6\mathrm{Be}_{g.s.}$ spectra from the ^{13}O data set with its much higher statistics [Fig. 6(d)]. More details of this R-matrix calculation can be found in Sec. V. Further evidence that peaks B, E, and H are branches of the same state is obtained from their fitted relative yields. Figure 7 shows the ratios of yields of peaks B and H relative to peak E obtained from the three data sets. These ratios are consistent between these data sets as expected for decay branches from a common state. While peaks A and D in the $p + {}^9\mathrm{B}_{g.s.}$ and $2p + {}^8\mathrm{Be}_{g.s.}$ channels are separated by only ≈65 keV, their ratio of yields (Fig. 7) varies significantly in the three data sets indicating that these two peaks are associated with two different levels in ^{10}C.

For the other peaks, centroids and widths were constrained from fits to the high-statistics ^{13}O data set where these higher-energy peaks are most prominent. The fitted spectra are shown in Figs. 4(b) to 4(e). Peak L in Fig. 4(d) is very wide and an R-matrix intrinsic lineshape for a single-channel was utilized. Unless an anonymously large channel radius is assumed, the wide width of this state cannot be reproduced with $\ell > 1$ giving the spin-parity possibilities listed in Table I. Again, many of the peaks in the different channels fall at the same energy and so these were also treated as decay branches of common parent states and the level parameters were obtained

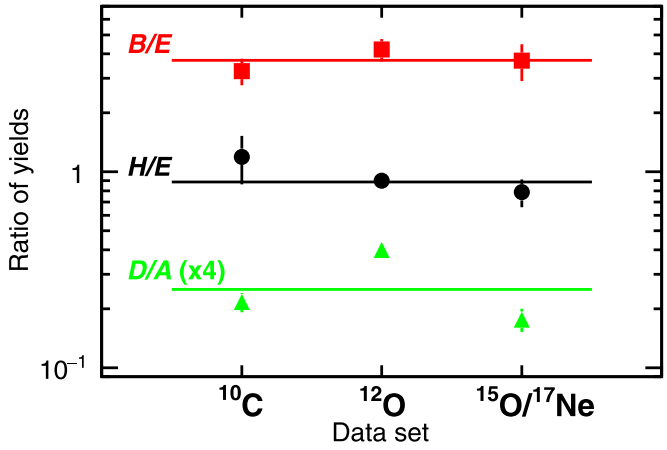

FIG. 7. Ratio of fitted yields of the specified peaks from the ^{10}C, ^{13}O, and ^{15}O / ^{17}Ne data sets. The horizontal lines give the weighted mean ratios from all three data sets.

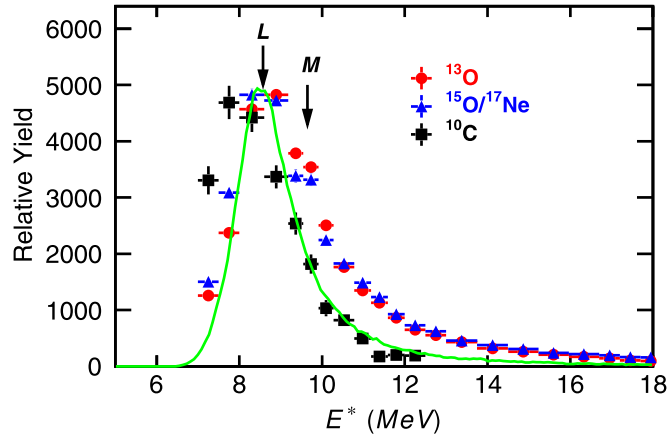

FIG. 8. Distribution of ^{10}C excitation energy for events which proton decay to the $5/2^-$ state in ^{9}B. Results are shown for three of the data sets considered in this work. The experimental data have been normalized to the same maximum value on the *y* axis. While the data for the ^{13}O and ^{15}O / ^{17}Ne data sets can be fit with contributions from peaks *L* and *M* [see Fig. 4(d) for the ^{13}O data set], the ^{10}C data cannot. For comparison, the curve shows the fitted contribution from peak *L* obtained from the ^{13}O data set. The addition of contributions from peak *M* would not improve agreement with the ^{10}C data.

from joint fits. Table I lists these decay branches and gives their fitted branching ratios. These have not been corrected for the detector efficiencies associated with the different decay branches as the momentum correlations between the decay products are not always known. The exception is for peaks *B*, *D*, and *H* were the correlations can be estimated, i.e., peak *B* is treated as a series of sequential steps with ^{9}B$_{g.s.}$ and ^{8}Be$_{g.s.}$ intermediate states; peak *E* undergoes prompt $2p$ decay with the proton momenta sampling the correlations measured from the ^{10}C data set in Ref. [21]; and peak *H* α decays to ^{6}Be$_{g.s.}$, which then $2p$ decays sampling the momentum correlations measured in Ref. [7].

We note that the simulated efficiencies for these three channels are quite different with peaks *B* and *E* having efficiencies of 5 and 2.4 times smaller than calculated for peak *H*, respectively. This is a result of the strong correlations associated with the decay of ^{8}Be$_{g.s.}$ and ^{9}B$_{g.s.}$ intermediate states which have small decay energies and thus their decay fragments are emitted with small relative angles. Typically more than one of these decay fragments enter the same CsI(Tl) crystal and the event is not identified. Such strong correlations are not expected for the other decay channels identified in this work and the efficiencies, for the same parent state, are expected to be more similar. With this in mind, the uncorrected branching ratio of 3.6(6)% for peak *G* associated with $2p$ decay to the ^{8}Be$_{g.s.}$intermediate would be expected to increase significantly if the correction could be made.

Figure 8 compares the $p + {}^9$B$_{5/2^-}$ spectrum obtained with the ^{13}O data set to those from the ^{10}C and ^{15}O / ^{17}Ne data sets where the latter two spectra have been normalized to give the same maximum peak height. Due to the lower statistics for the latter data sets, the spectra are now made with 400-keV-wide bins. The results for ^{15}O / ^{17}Ne data have largely the same shape implying similar relative contributions from the two peaks, *L* and *M*. However, the result from the ^{10}C data set is quite different peaking at a lower energy. Even if the contribution from the higher-energy peak *M* is missing in the ^{10}C data set, the observed distribution still peaks lower in energy than the fitted lineshape of peak *L* (green curve). This suggests that either there is another wide level associated with the $p + {}^9$B$_{5/2^-}$ channel or, more likely, the lower-energy inelastic-scattering reaction associated with the ^{10}C data set selectively populates the lower-energy part of the broad profile associated with resonance *L*.

A similar comparison between data sets is made for the $\alpha + {}^6$Be$_{g.s.}$ channel in Fig. 9 where now the spectra are normalized to give the same height for peak *I*. Peak *H* is clearly resolved in all data sets and evidence for peaks *I* and *J* is also seen in all sets. Peak *K*, which has a very small peak-to-background ratio in the ^{13}O data set, is not visible in the other two sets.

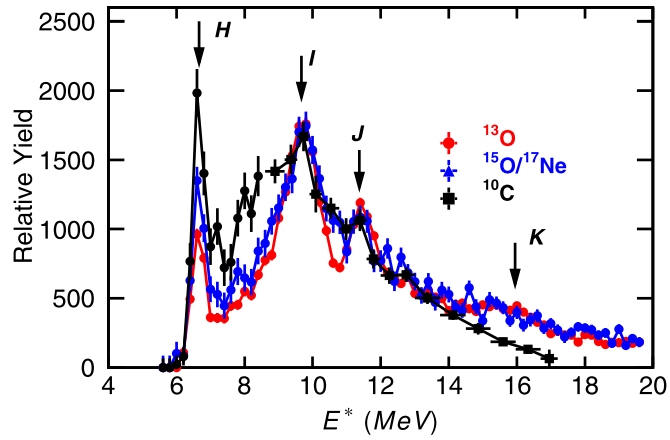

FIG. 9. Distribution of ^{10}C excitation energy for events which α decay to the ground state of ^{6}Be. Results are shown for three of the data sets considered in this work. The arrows indicate the location of fitted states tabulated in Table I. The results for each data set have been normalized to give the same peak maximum at 9.69 MeV.

For the ^{9}C data set where ^{10}C states are populated via neutron pickup reactions, peaks associated with ^{8}Be$_{g.s.}$ and ^{9}B$_{g.s.}$ intermediate states are relatively weakly populated [13]. This reaction is quite selective, largely populating the 9.647-MeV state, as seen in Fig. 4(f) where the two most intense branches *N* and *I* are observed. To a lesser extent, the 11.450-MeV state (peak *O*) is also observed. The peak-to-background ratio is much better for these states in this data set, but the statistics are smaller than the ^{13}O data set. The solid-red curves in Fig. 4(f) show fits to these spectra where the peak centroids and widths are constrained to the fitted values obtained from the ^{13}O data set. The overall reproduction of these spectra are good.

III. ^{11}N STATES DECAYING TO THE $3p + 2\alpha$ EXIT CHANNEL

In this section we discuss ^{11}N states populating the $3p + 2\alpha$ exit channel. Lower-energy states that populate the $p + ^{10}$C channel from the ^{13}O data set have been presented in Ref. [9]. The ^{9,10}C and ^{15}O / ^{17}Ne data sets have insufficient statistics for the $3p + 2\alpha$ channel and will be ignored. As for the $2p + 2\alpha$ events, the $3p + 2\alpha$ events can be subdivided into the same three groups. As the ground-state of ^{11}N is not well constrained, we plot distributions of the total decay energy E_T instead. The spectrum associated with a ^{9}B$_{g.s.}$ intermediate state is plotted in Fig. 10(b) and four peaks (*N*, *O*, *P*, and *Q*) are well resolved.

The solid-red curve shows a fit to this distribution with four Breit-Wigner intrinsic lineshapes (dotted-green curves) and a smooth background (dashed-blue curves). Again, the experimental resolution and efficiency were included via Monte Carlo simulations [24]. The background shown in this figure was parametrized as an inverse-Fermi function times a cubic polynomial in this figure and the fitted background has a rapid rise at around $E_T \approx 2.5$ MeV, possibility associated with an unresolved wider peak contributing along with the other background sources. However this background is not well defined under peaks *O* to *Q*, which overlap. If, instead, the background is parametrized with an inverse-Fermi function times a quadratic polynomial, the fitted background is found to be smaller and flatter and the fitted widths of peaks *O* to *Q* increased by factors from 1.5 to 3. The fitted centroids are less sensitive to the background parametrization, with the largest change of 50 keV for peaks *P* and *Q*. The fitted parameters for peak *N* have also very little sensitivity to background parametrization as there is little background in its vicinity.

The fitted centroids and widths of the four peaks are listed in Table II where the uncertainty from the background parametrization is included. In addition the excitation energy based on the ground-state energy determined in Ref. [9] from the same data set is also listed. With these new states, the level scheme of ^{11}N is displayed in Fig. 11 where the first known decay steps are indicated by the arrows.

For the subdivision of events with a ^{8}Be$_{g.s.}$ but no ^{9}B$_{g.s.}$ intermediate state, the invariant-mass spectrum in Fig. 10(a) (green triangular data points) is rather featureless with no resolved states.

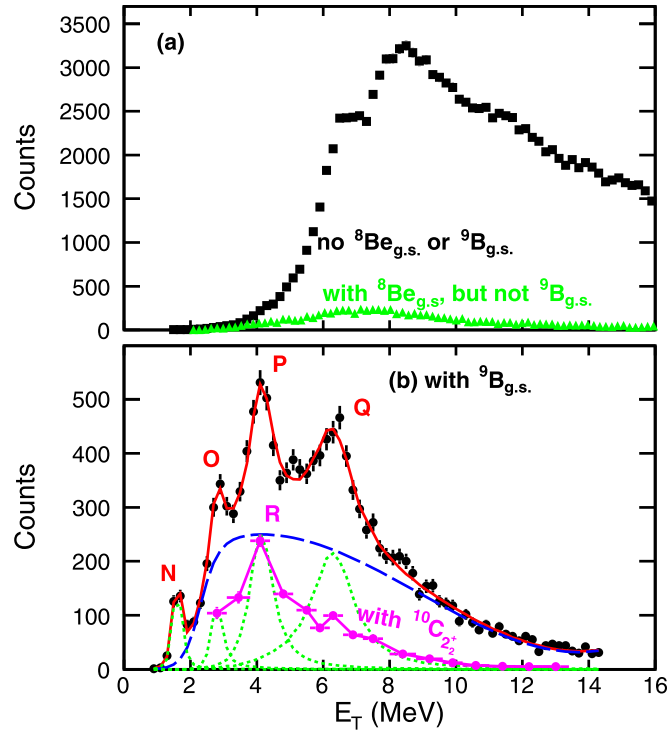

FIG. 10. Distributions of ^{11}N decay energy obtained from $3p + 2\alpha$ events with the invariant-mass method. Events which are associated with a ^{9}B$_{g.s.}$ are shown in panel (b), while those with no ^{9}B$_{g.s.}$, either with or without an ^{8}Be$_{g.s.}$ are shown in panel (a). The solid-red curve in panel (b) shows a fit to this data with a background (dashed blue curve) and four peaks (dotted green curves). The magenta data points in panel (b) indicated the yield associated with proton decay to the ^{10}C$_{2_2^+}$ intermediate state. Labels for peaks discussed in this work are shown.

Similar to the analysis of the $2p + 2\alpha$ events, those events without an ^{8}Be$_{g.s.}$ intermediate state can be analyzed to give the contributions from ^{9}B$_{5/2^-}$ and ^{6}Be$_{g.s.}$ intermediate states. The ^{11}N decay energy spectra for these events are plotted in Fig. 12. The result for the ^{6}Be$_{g.s.}$ intermediate state

TABLE II. Level parameters obtained from the fits to the $3p + 2\alpha$ invariant-mass spectra of Figs. 10(b) and 12. The intermediate states identified from the correlations are indicated. The excitation energy is based on the ground-state mass obtained from the same data in Ref. [9]. The uncertainties listed are statistical, in addition there is a systematic uncertainty of 10 keV in the centroids [9,24].

J_π	E_T [MeV]	E^* [MeV]	Γ [keV]	Peak	Intermediate state
$3/2^-_2$	1.588(18)	3.940(18)	136(24)	*N*	^{9}B$_{g.s.}$
$(5/2^-)$	2.774(40)	5.126(40)	492(239)	*O*	^{9}B$_{g.s.}$
$(7/2^-)$	4.081(104)	6.433(104)	836(338)	*P*	^{9}B$_{g.s.}$
				R	^{10}C$_{2_2^+}$
$(9/2^-)$	6.390(70)	8.742(70)	1770(356)	*Q*	^{9}B$_{g.s.}$
	6.919(58)	9.271(58)	1126(201)	*S*	^{9}B$_{5/2^-}$
	8.695(67)	11.047(67)	1825(239)	*T*	^{9}B$_{5/2^-}$

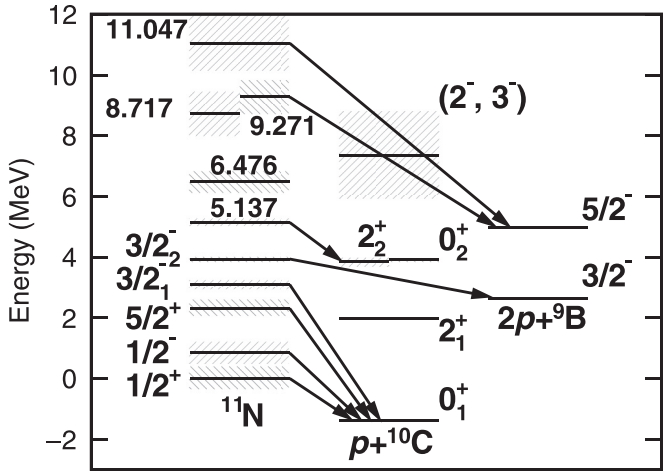

FIG. 11. Level scheme for ^{11}N states obtained in this work and from Ref. [9]. Where known, the first step in the decay of each level, either $1p$ or $2p$ emission, is indicated by an arrow.

[Fig. 12(a)] shows no prominent peaks, while one can resolve two peaks in the results for the $^{9}B_{5/2^-}$ intermediate state [Fig. 12(b)]. The solid curves show a fit to this spectrum with three contributing R-matrix lineshapes for diproton emission to $^{9}B_{5/2^-}$ [31]. Again the effect of the detector efficiency and resolution was included via Monte Carlo simulations. The higher-energy peak in the fit is not resolved in the experimental data and could in fact represent a background from multiple peaks and other sources. The two lower-energy peaks (S and T) are located at $E_T = 6.919(58)$ and 8.695(67) MeV with widths of 1.126(201) and 1.825(239) MeV, respectively.

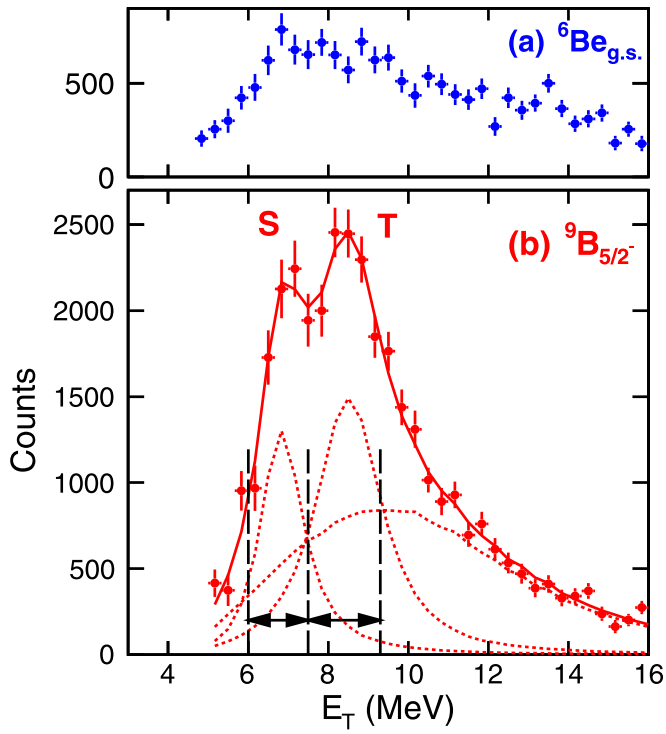

FIG. 12. Distributions of ^{11}N decay energy obtain from $3p + 2\alpha$ events which contained (a) a $^{6}Be_{g.s.}$ or (b) a $^{9}B_{5/2^-}$ intermediate state. The $^{9}B_{5/2^-}$ results have been fit (solid curves) with the sum of three ^{11}N peaks (dotted curves) where the detector efficiency and resolution have been incorporated via Monte Carlo simulations. Gates are indicated for which two-proton correlation plots are displayed in Fig. 16. Labels for the two peaks discussed in the text are given.

Finally for the subdivision of events which decay through $^{9}B_{g.s.}$, we can use a similar scheme to look for ^{10}C intermediate states by projecting the E_T values for $2p + 2\alpha$ subevents with gates on the ^{11}N invariant mass. Within the statistics, only the 2^+_2 excited state of ^{10}C could be identified. This intermediate state, of course, proton decays to the $^{9}B_{g.s.}$ state. The invariant-mass distribution associated with the $^{10}C_{2^+_2}$ state is shown by the magenta data points in Fig. 10(b) where one peak, labeled R is visible. This peak is at the same energy as peak P and thus represents one decay branch of a state at $E_T = 4.124$ MeV. It is possible that peaks O, P, and Q have branches from other ^{10}C intermediate states and there may also be yield associated with prompt $2p$ emission directly to $^{9}B_{g.s.}$. Peak N, the lowest-energy of the ^{11}N peaks, decays predominantly by prompt two-proton emission and is discussed in Sec. IV B.

IV. $2p$ DECAY

Before considering prompt $2p$ decay of excited states in ^{10}C and ^{11}N, let us briefly review prompt $2p$ decay from ground states. Ground-state $2p$ decay has been observed from a number of even-Z nuclides ranging from ^{6}Be to ^{67}Kr [32]. The lightest cases, ^{6}Be, ^{11,12}O, and ^{15,16}Ne are associated with democratic $2p$ decay where there exists a wide intermediate state (the $Z-1$, $A-1$ ground state) [1]. The complete momentum correlations in $2p$ decay can be represented by a two-dimensional distribution [33] which has only been measured with high statistics for three ground-state emitters, i.e., the democratic decays of $^{6}Be_{g.s.}$ [7], $^{12}O_{g.s.}$ [9], and $^{16}Ne_{g.s.}$ [23]. The next-best case is for ^{45}Fe where the correlations were extracted from 75 events [3,34]. Theoretical studies show that the correlations are determined by the initial-state nuclear structure modified by the decay dynamics and final-state interactions [3,7,22,33,35].

Comparison of the correlations between different emitters is most easily made via their one-dimensional projections. In this work we consider projected distributions on the quantities $E_{\text{core-}p}/E_T$ and $E_{p\text{-}p}/E_T$, where $E_{\text{core-}p}$ is the relative energy between one of the protons and the core and $E_{p\text{-}p}$ is the relative energy between the two protons. These are complementary variables and give information on different aspects of the system. For the former, there are two possible values for each $2p$ decay and both are used to increment the presented distributions.

A comparison of the projected correlations for $^{6}Be_{g.s.}$, $^{12}O_{g.s.}$, and $^{16}Ne_{g.s.}$ obtained from Refs. [7,9,23] is shown in Fig. 13 where these distributions are indicated by the dotted curves and are normalized to the same total yield. These decays are from 0^+ initial states to 0^+ final states and hence the two protons remove no net angular momentum. In addition, these $2p$ emitters have quite similar decay energies $Q_{2p} = 1.37$-1.72 MeV which are listed individually in the

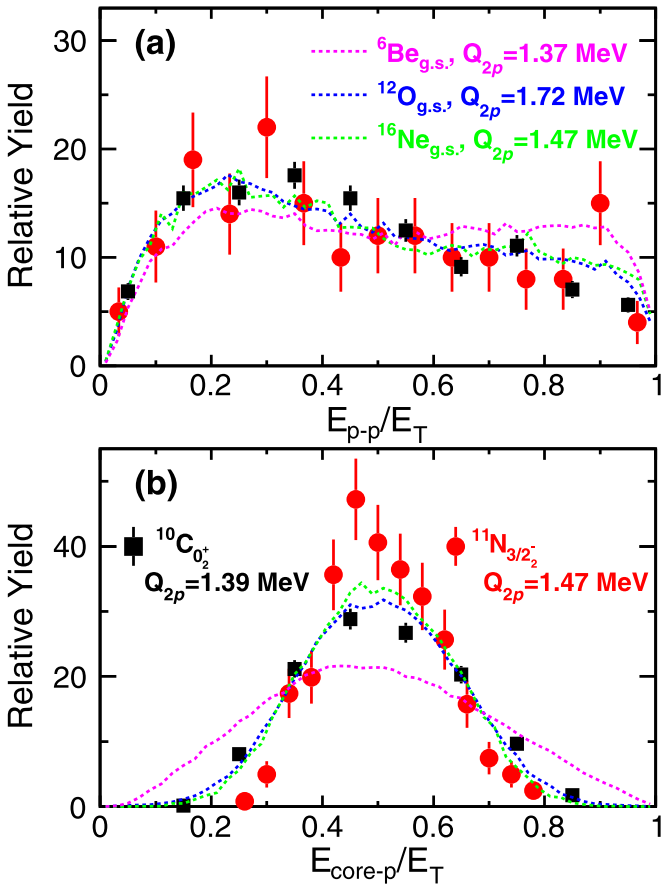

FIG. 13. Correlation plots (data points) for the two-proton decay of the $^{11}N_{3/2_2^-}$ (red) and $^{10}C_{0_2^+}$ (black) states. Panel (a) shows the relative p-p energy while panel (b) shows the p-core relative energy. For comparison, experimental results from the ground-state two proton decay of ^{6}Be, ^{12}O, and ^{16}Ne are displayed as the dotted curves. Each data set was normalized to give the same integrated yield.

figure. The correlations for ^{12}O and ^{16}Ne are almost identical and the $E_{p\text{-}p}/E_T$ distribution for ^{6}Be is not very different from those of the heavier $2p$ emitters.

Prompt emission of two protons from the same single-particle orbital is expected to be characterized by $E_{\text{core-}p}/E_T \approx 0.5$, i.e., the two proton are emitted with similar kinetic energies as this maximizes the product of their barrier penetration factors for a fixed total decay energy. This feature is demonstrated in Fig. 13(b) in all the experimental distributions. The distribution for ^{6}Be is wider than the two heavier ground-state emitters. As the charge of the α core in ^{6}Be is small, the Coulomb focusing to $E_{\text{core-}p}/E_T \approx 0.5$ is not as strong in this case. In addition as the core is also very light, recoil effects will be larger for ^{6}Be. The $E_{p\text{-}p}/E_T$ quantity is closely related to the relative angle between the emitted protons, with small relative energies and angles often called diproton-like and large values associated with back-to-back proton emissions sometimes referred to as cigar configurations.

Different single-particle configurations of the two valence protons give rise to different relative-angle distributions inside the nucleus. For instance, the $[s_{1/2}]^2_{J=0}$ and $[p_{1/2}]^2_{J=0}$ configurations have isotropic distributions, while the $[p_{3/2}]^2_{J=0}$ configurations have significant diproton and cigar correlations. In principle there can be more than one configuration which would make the relative angle distributions more complex due to interference effects. In Ref. [9] it was argued that the similarity of the E_{p-p}/E_T distributions for ^{12}O and ^{16}Ne emitters is due to the fact that these decays are dominated by the $[1s_{1/2}]^2_{J=0}$ component. For instance, with an initial wave function of ^{12}O with 36% $[s_{1/2}]^2_{J=0}$, 25% $[0p_{1/2}]^2_{J=0}$, and 14% $[0d_{5/2}]^2_{J=0}$ [5], a time-dependent calculation of its decay by Wang and Nazarewicz showed that the $[s_{1/2}]^2_{J=0}$ component accounted for 73% of the emitted proton pairs [35]. The initial wave function of ^{16}Ne is also expected to have a significant $[1s_{1/2}]^2_{J=0}$ component with predictions of 45(5)% [36] and 50%–75% [37] with most of the remaining strength being $[0d]^2_{J=0}$. As the decay of the latter is greatly suppressed by barrier penetration, the ^{16}Ne decay should also be dominated by $[1s_{1/2}]^2_{J=0}$ emission.

Unlike the ^{12}O and ^{16}Ne nuclides, the internal wave function for ^{6}Be is not expected to have significant $[1s_{1/2}]^2_{J=0}$ strength but should be dominated by the $[0p_{3/2}]^2_{J=0}$ component instead. However, theoretical calculations indicate that this component mixes with the $[1s_{1/2}]^2_{J=0}$ configuration during the barrier-penetration phase [22,33,35]. The final observed distribution is predicted to have roughly equal contributions from both $[0p_{3/2}]^2_{J=0}$ and $[1s_{1/2}]^2_{J=0}$ configurations, which explains its similarity to the $[1s_{1/2}]^2_{J=0}$ dominated $E_{p\text{-}p}/E_T$ distributions for ^{12}O and ^{16}Ne. The most significant difference in the $E_{p\text{-}p}/E_T$ distributions between ^{6}Be and the heavier emitters is in the region near back-to-back emissions, where the $[0p_{3/2}]^2_{J=0}$ component is relatively stronger in the former. These measured correlations can serve as templates to identify $2p$ emission with no net angular momentum removal in light nuclei located in the p and sd shells, although care should be taken for much smaller or larger decay energies. For heavier systems we note that the $E_{p\text{-}p}/E_T$ distribution for ^{45}Fe in Ref. [3,34] is much different to those in Fig. 13 as very little $[1s_{1/2}]^2_{J=0}$ component [38] is expected.

A. 0_2^+ state of ^{10}C

Fortune and Sheer predict the second 0^+ state in ^{10}C has a configuration of an ^{8}Be core coupled to two protons in the sd shell and its decay via p-wave emissions is very small [39]. In particular, their calculations indicate it has a large $[s_{1/2}]^2_{J=0}$ component and thus we may observe its $2p$ decay to ^{8}Be. This decay would be democratic because there exists a wide intermediate state, the $1/2^+$ first-excited state of ^{9}B, which is expected to be an s-wave resonance. See Fig. 14 for the energy of this state relative to the initial and final states. We have used the ENSDF values for the $^{9}B_{1/2^+}$ state [30] in this plot, but note that its energy and width are not well determined [40].

The two-dimensional momentum correlations between the three decay fragments in the $2p$ decay of ^{10}C to ^{8}Be$_{g.s.}$ for peaks D and E were presented from the ^{10}C data set in Ref. [15]. We will first concentrate on the peak D which was tentatively assigned as the 0_2^+ state in that reference. The correlations for peak E will be discussed later. The ^{10}C data set is preferred for these correlations as, while the counting

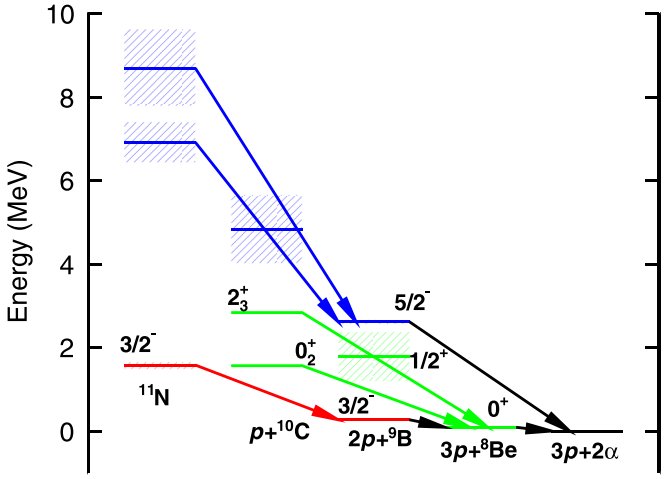

FIG. 14. Level diagram showing the states in ^{11}N and ^{10}C associated which $2p$ decay and states of interest in their decay. For each $2p$ emitter, the initial, wide intermediate state, and $2p$-residual states are shown in the same color.

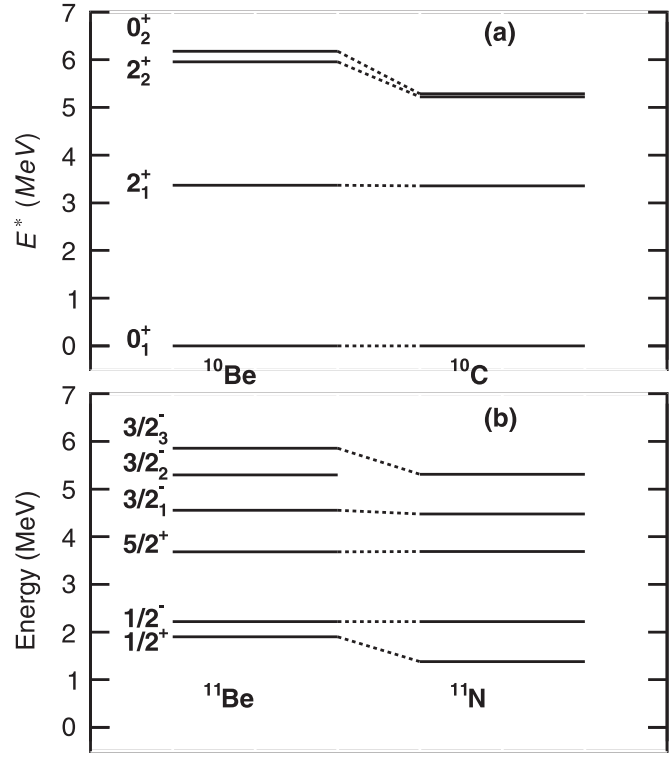

FIG. 15. Level schemes for the mirror pairs (a) ^{10}Be - ^{10}C and (b) ^{11}Be - ^{11}N, showing the Thomas-Ehrman shifts for the second 0^+ state in panel (a) and the second $3/2^-$ state in panel (b). The energies of the levels in ^{11}N are given relative to the $p+{}^{10}$C threshold, whereas for ^{11}Be we have shifted them so that $1/2^-$ state lines up with its analog in ^{11}N.

statistics are not the largest, the peak-to-background ratio and invariant-mass resolution are the best of all the data sets.

Since the original measurement of these ^{10}C correlations, momentum correlations associated with the democratic $2p$ decay of ^{6}Be [7], ^{12}O [26], and ^{16}Ne [23] 0^+ ground states to 0^+ residual states have been measured and we now compare these to the ^{10}C* correlations in Fig. 13 where the results for the peak D are shown by black-square data points. This is a useful comparison as the $2p$ decay energy of this state to ^{8}Be is $Q_{2p} = 1.466(50)$ MeV which is comparable to those for the ground-state emitters which are listed in the figure. As expected for $2p$ decay, the $E_{\text{core-}p}/E_T$ distribution is peaked at 0.5. More importantly, the correlations are almost identical to the ^{12}O$_{\text{g.s.}}$ and ^{16}Ne$_{\text{g.s.}}$ results which are dominated by $[1s_{1/2}]^2_{J=0}$ emission. This suggests that the decay of this ^{10}C state also has a substantial $[1s_{1/2}]^2_{J=0}$ component which fixes its spin as 0^+.

The $E_{p\text{-}p}/E_T$ distribution for this ^{10}C state is closer to the ^{12}O and ^{16}Ne results than the ^{6}Be data and thus we conclude that the $[1s_{1/2}]^2_{J=0}$ component is likely associated with the initial wave function and not due to the effect of the decay dynamics as in ^{6}Be. With a significant $[1s_{1/2}]^2_{J=0}$ component, we expect to see a sizable Thomas-Ehrman shift between the energy of this level and its analog in ^{10}Be. The levels of the mirror pair are compared in Fig. 15 and indeed both the 0^+_2 and 2^+_2 levels have Thomas-Ehrman shifts. The latter is probably due to a $[1s_{1/2}, 0d_{5/2}]_{J=2}$ configuration. For the 0^+_2 state, Fortune and Sherr predict a Thomas-Ehrman shift of 1.00(11) MeV [39] which is very close to the value of 0.892(15) MeV obtained in this work.

The partial width for p-wave decay to ^{9}B$_{\text{g.s.}}$ is predicted to be very small (4^{+4}_{-2} keV) by Fortune and Sherr [39]. Experimentally such a decay branch would lie in our first subdivision of the $2p+2\alpha$ events and should be found in the invariant-mass distributions of Fig. 2(a). We see no evidence of such a branch, but our sensitivity is reduced as, at this energy, the invariant-mass spectra are dominated by the peaks associated with the more intense 2^+_2 state (peak A). We place a 70% upper limit on this $p+{}^9$B$_{\text{g.s.}}$ branching ratio at the 2σ level by fitting the spectra in Fig. 2(a) with an extra peak of the same energy and width as peak D in addition to observed peaks.

B. $3/2^-_2$ state of ^{11}N

Fortune has predicted an excited $3/2^-$ state in ^{11}N with two protons in the sd shell coupled to a ^{9}B$_{\text{g.s.}}$ core [41]. The predicted partial decay widths for p-wave emissions to the ground and first-excited states in ^{10}C were small and so we also consider whether this state will decay to ^{9}B$_{\text{g.s.}}$ via $2p$ emission. The candidate for this state is peak N, the lowest of the resolved states in Fig. 10(b). The fitted width for this state of 136(24) keV makes it the narrowest ^{11}N state known.

Its momentum correlations (red data points) are compared with the ground-state systematics in Fig. 13. We again note that its $2p$ decay energy of $Q_{2p} = 1.303(12)$ MeV is comparable to the values for the ground-state systematics and that the $E_{p\text{-core}}/E_T$ distribution is peaked near 0.5 as expected for $2p$ decay. Its correlations are also very similar to the ^{12}O$_{\text{g.s.}}$ and ^{16}Ne$_{\text{g.s.}}$ results, indicating a significant $[1s_{1/2}]^2_{J=0}$ decay component and thus its spin is $3/2^-$. The statistical error bars are larger in this case and it is possible that the $E_{p\text{-}p}/E_T$

distribution is consistent with the ^{6}Be result where the $[1s_{1/2}]^2_{J=0}$ component is a result of the decay dynamics rather than the initial wave function.

However, if the initial wave function has a significant $[1s_{1/2}]^2_{J=0}$ component, then we would expect to see a Thomas-Ehrman shift relative to its analog in ^{11}Be. Care must be taken in accessing the magnitude of the Thomas-Ehrman shift as the $1/2^+$ ground state of ^{11}N is expected to be an s-wave resonance [42] and a consistent centroid has not been found in experimental studies. In Fig. 15(b), the known levels as listed in Ref. [9], plus the results of this work, are plotted at their energy above the $p + {}^{10}$C threshold. The analog levels in the mirror nucleus ^{11}Be from the ENSDF data base [30] have been shifted so that the $1/2^-$ first-excited states line up. With this shift, the second and third excited states also approximately line up and the ground states shows a significant Thomas-Ehrman shift as expected. The ENSDF data base lists three $3/2^-$ states in ^{11}Be within an interval of 1.5 MeV, as seen in Fig. 15(b). This leaves the question as to whether our second observed $3/2^-$ in ^{11}N is the analog of the second or third $3/2^-$ ^{11}Be level in the ENSDF data base. However, we note that some studies suggest that the second-listed $3/2^-$ state is actually $J^\pi = 3/2^+$ [43,44]. Fortune has identified the third listed $3/2^-$ state in ^{11}Be as the one with large sd configuration strength [41]. With this assignment, we find a Thomas-Ehrman shift of 0.542(12) MeV which is 62% of the shift measured for the 0^+_2 state of ^{10}C and implies a smaller $[1s_{1/2}]^2_{J=0}$ component.

Relative to this same reference state, Fortune's predictions imply a Thomas-Ehrman shift of 1.07 MeV. This predicted shift is associate with a $[1s_{1/2}]^2_{J=0}$ component with a strength of 84%. However, Fortune notes that, alternatively, a $[1s_{1/2}, 1d_{5/2}]_{J=2}$ component could give to rise a similar shift. In any case, the predicted shift is too large and also points to the delicate balance involved in terms of the amount of $[1s_{1/2}]^2_{J=0}$ component. One might expect that by increasing this component it increases the $2p$ decay probability, but in the work of Fortune this results in a large Thomas-Ehrman shift which reduces the $2p$ decay energy to 0.78 MeV, significantly less than the experimental value of 1.303(12). The penetration factor for the emission of two protons changes rapidly with decay energy and a change of this magnitude would greatly suppress $2p$ emission.

The magnitude of this suppression depends on the competing decay branches. Fortune indicates that single-proton p-wave decay to the 2^+_1 first-excited state of ^{10}C should dominate these competing branches with a partial width of $\approx$70 keV. The total width, extracted from the fitting of the invariant-mass spectra, is 136(4) keV suggesting a $2p$ decay width of $\approx$60 keV with two decay branches of similar magnitude. This $1p$ decay branch should populate the $p + {}^{10}$C invariant-mass spectrum at $E_T = 1.957(12)$ MeV after removing the energy of the γ-ray which deexcites the 2^+_1 state in ^{10}C. This spectrum is shown in Fig. 4(b) in Ref. [9], but unfortunately the contribution from this decay branch lies under the peak associated with the $1/2^-$ first-excited state of ^{11}N which dominates the spectrum. Thus we are not very sensitive to this decay branch. Fits to the $p + {}^{10}$C invariant-mass spectrum, when adding an extra peak for this state, gives a maximum limit to the $1p$ branching ratio to the 2^+_1 state of 40% at the 2σ level which is close to Fortune's estimate.

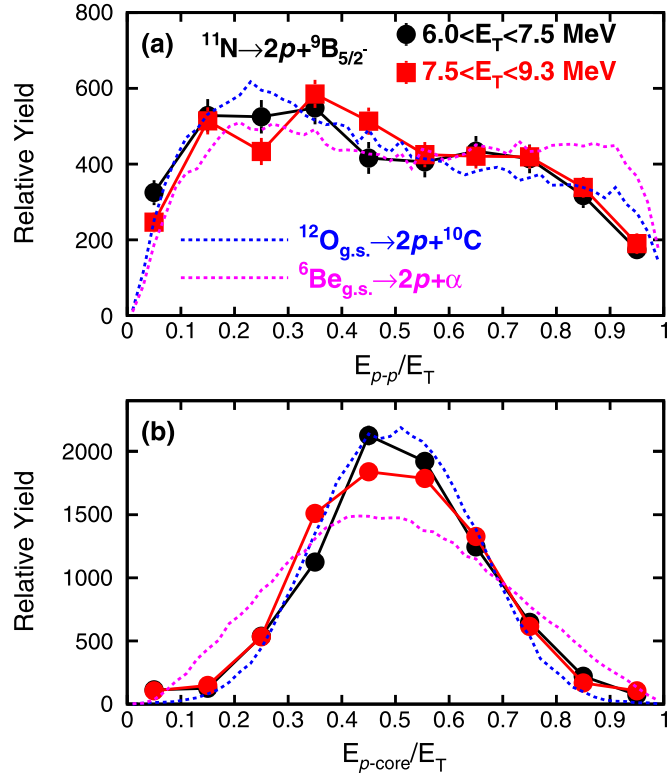

FIG. 16. Correlations plots (data points) for the two-proton decay of ^{11}N states to a ^{9}B$_{5/2^-}$ residual. Results are shown for the two gates indicated in Fig. 12 centered around the fitted ^{11}N peaks. These results are compared with correlations associated with two-proton decay from the ground states of ^{12}O and ^{6}Be from Refs. [7,26]. Each data set was normalized to give the same integrated yield.

If we consider the $2p$ decay of this ^{11}N excited state as a democratic $2p$ decay, like the 0^+_2 state of ^{10}C and the ground states of ^{6}Be, ^{12}O, and ^{16}Ne, then there should exist a wide intermediate state in ^{10}C. No such state is known experimentally. If like in these democratic $2p$ emitters the intermediate state is an s-wave resonance, then its spin would be 1^- or 2^-. States of this spin exist in the mirror nucleus ^{10}Be at the appropriate excitation energies, but their analogs in ^{10}C have yet to be identified.

C. Peaks S and T in ^{11}N

Peaks S and T located at $E^* = 9.271$ and 11.047 MeV ($E_T = 6.919$ and 8.695 MeV) were found to decay though the $5/2^-$ state in ^{9}B and must be considered as democratic $2p$ emitters. The only possible intermediate state in ^{10}C that decays through ^{9}B$_{5/2^-}$ is the wide peak L at $E^* = 8.4$ MeV which is an s or p-wave resonance. Figure 14 shows the location of this intermediate state relative to the initial ^{11}N states and the $5/2^-$ state in ^{9}B.

The correlations for these states are compared with the ^{12}O and ^{6}Be ground-state results in Fig. 16. The experimental correlations were determined for the gates on E_T shown in

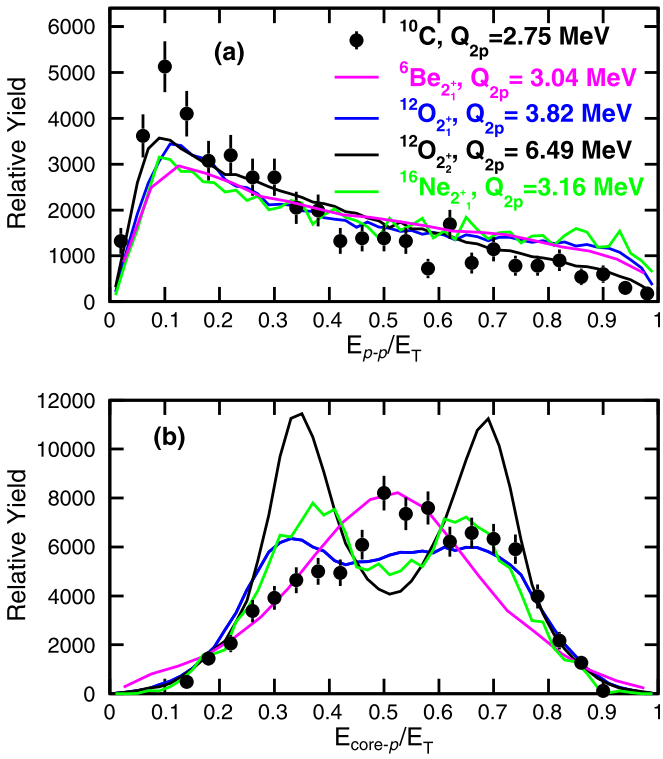

FIG. 17. Correlations plots (data points) for the two-proton decay of peak E obtained from the ^{10}C data set. These correlations are compared with experimental two-proton correlations from known 2^+ states from Ref. [7–9] shown by the solid curves. The $2p$ decay energies for each state are listed.

Fig. 12(b) and from the fit we can see that they are not entirely clean because these states overlap and there is significant background under the fitted peaks. The $E_{\text{core-}p}/E_T$ distributions are peaked near 0.5 as expected for prompt $2p$ emission and, surprisingly, the correlations are almost identical to each other and to those obtained for ^{12}O$_{\text{g.s.}}$ which might suggest that they are dominated by $[1s_{1/2}]^2_{J=0}$ emission. However one should be very cautious here, the $2p$ decay energy for these two states are $Q_{2p} = 4.235(49)$ and 6.011(68) MeV, respectively, much greater than the value of $Q_{2p} = 1.718(15)$ for ^{12}O, so if there is a strong Q_{2p} dependence on the $[1s_{1/2}]^2_{J=0}$ correlation, this comparison will be misleading. Further work is needed to understand the structure of these states.

D. 2_3^+ state in ^{10}C

A second state in ^{10}C which $2p$ decays to ^{8}Be$_{\text{g.s.}}$ is peak E. Its correlations, shown as the data points in Fig. 17, are different to the other momentum correlations considered so far as there is a strong enhancement of small $E_{p\text{-}p}$ values, i.e., diproton-like emissions. Similar enhancement has been observed in $2^+ \rightarrow 0^+$ $2p$ decays as shown in Fig. 17 which compares the ^{10}C correlations to known $J^\pi = 2^+$ $2p$ emitters in ^{6}Be, ^{12}O, and ^{16}Ne [7–9]. The $E_{p\text{-core}}/E_T$ distributions show an evolution from a single peak centered at 0.5 typical of ground-state $2p$ emitters to bi-modal distributions one would expect to find in sequential-decay scenarios. However, the

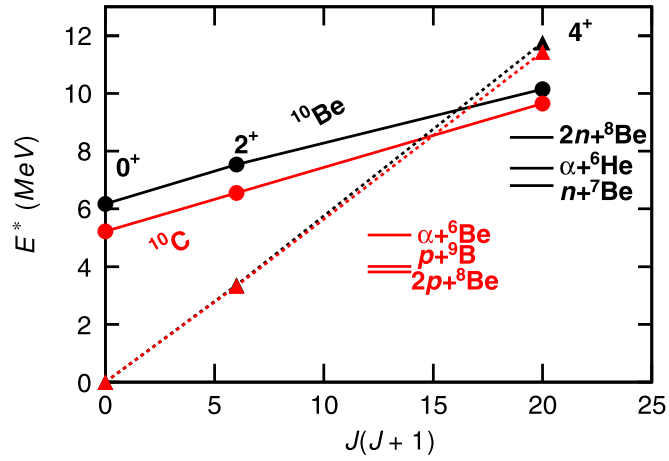

FIG. 18. Spin dependence of rotational bands in the mirror nuclei ^{10}Be (black) and ^{10}C (red). The levels for ^{10}Be are taken from Refs. [19,49,50]. The levels for the excited band in ^{10}C and the 4^+ member of the ground-state band are assigned from this work. Thresholds are shown for the decay channels of interest in both mirror nuclei. The dotted and solid lines connect the data points from the ground-state and excited 0^+ bands, respectively.

$E_{p\text{-}p}/E_T$ distributions are not consistent with sequential decay and show little variation among the different 2^+ states with strong diproton-like peaks similar to that found for peak E in ^{10}C. This enhancement of the diproton-like decay can be considered as a fingerprint for $2^+ \rightarrow 0^+$ decays, at least in this mass region. However theoretical studies are needed to understand the preference for diproton-like emissions and the evolution of the $E_{p\text{-core}}$ distributions. From the comparison in Fig. 17 we associated peak E with the $2p$ decay of a 2^+ state in ^{10}C, the third-known 2^+ state in this isotope. This state also has α and $1p$ decay branches (Table I).

V. DISCUSSION

The cores of the $2p$ emitters investigated in this work, ^{8}Be$_{\text{g.s.}}$, ^{9}B$_{\text{g.s.}}$, and ^{9}B$_{5/2^-}$ all have strong α-cluster structure. The ^{9}B$_{5/2^-}$ state is often considered as the second member of the $K^\pi = 3/2^-$ ground-state rotational band. Additionally, the analog of the 0_2^+ state in ^{10}Be is considered a cluster state, the bandhead of a rotational band [45,46] with the two valence neutrons located in σ molecular orbits. Similarly, the analog of the $3/2^-$ state in ^{11}Be has been tentatively assigned as a cluster state, the bandhead of a $K^\pi = 3/2^-$ rotational band [17,47,48]. Thus the extent of α clustering in the observed ^{10}C and ^{11}N states should be considered.

A. α-cluster states in ^{10}C

Figure 18 compares both ground-state and 0_2^+ rotational bands in the mirror nuclei ^{10}Be and ^{10}C where we have added spin assignments to some of the states discussed in this work. The α-cluster states in ^{10}Be were identified in Refs. [19,49,50]. For the second member of the 0_2^+ band in ^{10}C, we have assigned the 2_3^+ excited state associated with peaks B, E, and H. Like the 0_2^+ bandhead, this state also has a

$2p$ decay branch. In addition as this state is above the α-decay threshold, we see the significant α decay branch expected for an α-cluster structure. The slope of the rotation curve between the assigned 0^+ and 2^+ states in Fig. 18 is similar to that for the mirror, suggesting they have very similar moments of inertia. The next $J^\pi = 4^+$ member of this rotational band is tentatively assigned to the 9.647-MeV state associated with peaks *N*, *I*, *M*, and *G*. Like its lower 2^+ member, this state has $2p$ and α decay branches. However, the strongest decay branch listed in Table I is "other," i.e., unknown. With the larger spin, we would expect both $2p$ and α decays to the 2^+ excited states in ^{8}Be and ^{6}Be to contribute to this "other" category. However these intermediate states are wide making it impossible to separate these decay branches and isolate them from other possible decay paths. The choice of this state for the 4^+ member also maintains the same slope of the rotational curve in Fig. 18 consistent with the ^{10}Be counterpart.

The 2^+ second member of the ground-state rotational band is the well-known first-excited state of ^{10}C at $E^* = 3.353$ MeV [30]. The 4^+ member of the mirror ^{10}Be ground-state rotational band is plotted as the 11.76 MeV state following the suggestion of Hamada *et al.* [49]. Our 11.450 MeV state is a good candidate for its analog in ^{10}C. It is interesting that our two assigned 4^+ states are the levels which are selectively excited in the neutron pickup reactions associated with the ^{9}C data set [Fig. 4(f)]. Transfer of nucleons to low-ℓ orbitals is suppressed for fast beams due to energy and momentum mismatch [51]. To produce 4^+ states, the neutrons must be transferred to $\ell = 3$ or 5 single-particle orbits, which are relatively high ℓ for such a light nucleus. This helps ameliorate the suppression due to the energy and momentum mismatch. However, these states must still have some non-negligible $n + {}^9$C strength for them to be observed in the pickup reactions.

Arguments for assigning the 2^+ and 4^+ members of the 0^+_2 band in ^{10}Be were based on the reduced width γ^2_α for α decay [19,52]. For the 2^+ state of this band, taking the weighted mean of the $\alpha + {}^6\mathrm{He}_{\mathrm{g.s.}}$ branching ratios from Refs. [50,52] and the tabulated total decay width [30], the partial decay is $\Gamma_\alpha = 14.5(37)$ keV. With a standard channel radius of $a_\alpha = 1.6$ fm $\times (A_1^{1/2} + A_2^{1/3})$, the reduced width is $\gamma^2_\alpha = \frac{\Gamma_\alpha}{2P_2} = 0.56(25)$ MeV where P_2 is the $\ell = 2$ barrier penetration factor. This reduced width is quite large and close to the Wigner limit [53] of $\gamma^2_{\alpha W} = \frac{3\hbar^2}{2\mu a_\alpha^2} = 0.88$ MeV. For the analog state in ^{10}C assigned in this work, we obtain $\gamma^2_\alpha = 0.16(7)$ MeV from a similar analysis using the total decay width and branching ratio from Table I. Alternatively using the more precise total width measurement of $\Gamma = 190(35)$ keV from Ref. [54], we obtain $\gamma^2_\alpha = 0.17(3)$ MeV. These values are still significant, but are below the value for the analog state. For the three observed decay channels of this ^{10}C state, the dimensionless reduced decay widths are $\gamma^2_p/\gamma^2_{pW} = 0.03(1)$, $\gamma^2_{2p}/\gamma^2_{2pW} = 0.09(4)$, and $\gamma^2_\alpha/\gamma^2_{\alpha W} = 0.19(9)$, where the $2p$ decay is treated as the emission of a diproton with decay energy of $E_{p\text{-}p} = 0.9$ MeV which is the average $E_{p\text{-}p}$ value in Fig. 17(a). Of these channels, α decay is the strongest, consistent with an α-cluster structure of the internal wave function.

Let us now turn our attention to the 4^+ members in these analog 0^+_2 rotational bands. From the partial $\alpha + {}^6\mathrm{He}_{\mathrm{g.s.}}$ decay width of $\Gamma = 0.13(1)$ MeV [19], the reduced width of the 4^+_1 state in ^{10}Be is $\gamma^2_\alpha = 0.15(1)$ MeV close to the value for the 2^+ state in ^{10}C. For the proposed 4^+ analog state in ^{10}C, using the branching ratio uncorrected for detector efficiency in Table I, we obtain $\gamma^2_\alpha = 0.10(2)$ MeV. Of course the efficiency correction is unknown providing some extra uncertainty to this result, but we see the reduced decay width is of similar magnitude to its analog. Thus the α decay widths of these 2^+ and 4^+ states in ^{10}C support our contention that they are members of the 0^+_2 rotational band.

From an extrapolation of the lower-energy members using the best-fit momentum of inertia, we expect the 6^+ member of this 0^+_2 band in ^{10}C to lie at $E^* \approx 14.5$ MeV. The 15.95-MeV state is closest to this expectation. However for a spin of 6^+, its reduced α-decay width would be only $\gamma^2_\alpha = 0.024(6)$ MeV without correcting for detector efficiencies. The detector-efficiency corrections are unlikely to significantly increase this value bringing it closer to those obtained for the 2^+ and 4^+ states. Thus this state is probably not the 6^+ member and we would expect the real 6^+ state is probably quite wide making it difficult to observe.

B. α-cluster states in ^{11}N

The case for the α-cluster structure of the $3/2^-_2$ state in ^{11}N should also be considered. In the mirror nucleus ^{11}Be, Bohlen *et al.* have tentatively assigned members of the $K = 3/2^-$ band up to spin $19/2^-$ [47] though definite spin assignments have only been made for the first two members. The moment of inertia of this tentative band is quite large consistent with α-cluster structure. However from a theoretical study, Descouvemont suggested the $3/2^-$ and $5/2^-$ states do not have α-cluster structure [55]. But assuming that there is a $K = 3/2^-$ band, can we assign excited members from this work to the ^{11}N counterpart? If, like the 0^+_2 band in ^{10}C, the lower members would all have two-proton decay branches, then these states should show up in the $2p + {}^9\mathrm{B}_{\mathrm{g.s.}}$ invariant-mass spectrum of Fig. 10(b) where three other peaks (*O*, *P*, and *Q*) in addition to the $3/2^-$ state are observed. Assuming these are all members of the $K = 3/2^-$ band, we compare their rotational curve to that given by Bohlen *et al.* for ^{11}Be in Fig. 19. The degree of overlap of the two tentative bands is remarkable. We note that the presence of these peaks in the $2p + {}^9\mathrm{B}_{\mathrm{g.s.}}$ invariant-mass distribution does not guarantee they has a prompt $2p$ decay branch as sequential decays through ^{10}C intermediate states are possible and indeed the $E^* = 7.476$-MeV state has some $p + {}^{10}\mathrm{C}_{2^+_2}$ branch (peak *R*). The higher members are above the α-decay threshold, but identifying the $\alpha + {}^7$B decay is almost impossible given the large $^7\mathrm{B}_{\mathrm{g.s.}}$ decay width of $\Gamma = 0.8$ MeV [30]. Although the data is quite suggestive, further work is needed to shore up these tentative α-cluster bands in both ^{11}Be and ^{11}N.

C. $2n$ decay of neutron-rich cluster configurations

Given the observation of $2p$ decay from the proton-rich α-cluster configurations, one may consider the possibility of $2n$

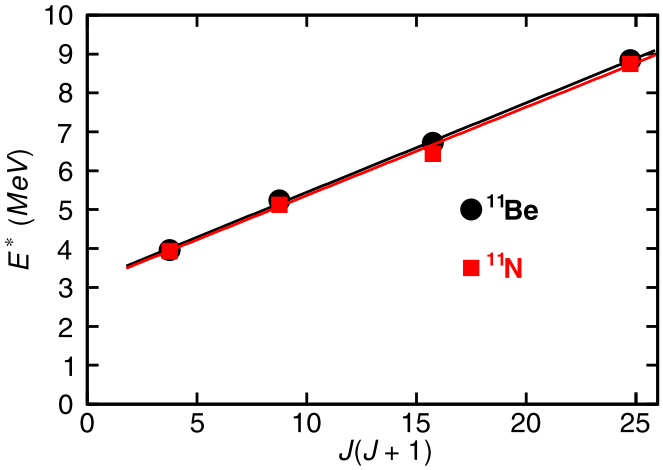

FIG. 19. Spin dependence of tentative $K = 3/2^-$ rotational bands in the mirror nuclei ^{11}Be and ^{11}N. The levels for ^{11}Be are taken from Bohlen *et al.* [47], while the levels for ^{11}N are those observed in the $2p + {}^9\mathrm{B}_{\mathrm{g.s.}}$ spectrum of this work. The red and black lines, which almost completely overlap, are fits to the two sets of levels.

decay of their neutron-rich cousins. In Fig. 18, where the ^{10}Be and ^{10}C rotational bands are displayed, we have also shown the thresholds for p, $2p$, and α decay of ^{10}C and their analogs for the neutron-rich counterparts. The 0^+ and 2^+ states in the ^{10}Be 0_2^+ band are below the $2n$ decay threshold thus leaving the 4^+ state as the first possibility for $2n$ decay in ^{10}Be. Note the $2p$ threshold is below the α threshold for ^{10}C, while the $2n$ threshold is above the α threshold for ^{10}Be. The energetics for $2n$ decay would be more favorable in ^{12}Be where $^6\mathrm{He} + {}^6\mathrm{He}$ and $\alpha + {}^8$He decays of molecular states have been observed [18,56,57]. The thresholds for these decays, 10.1 and 8.9 MeV, respectively, are quite large compared with the $2n$ decay threshold of 3.7 MeV.

VI. CONCLUSIONS

Highly fragmented decay channels of ^{10}C and ^{11}N excited states have been studied using invariant-mass data from four previous experiments involving both inelastic scattering, multinucleon knockout, and neutron-pickup reactions. For the $2p + 2\alpha$ exit channel, states in ^{10}C could be separated by gating and vetoing on the ground states of ^{8}Be and ^{9}B observed in the invariant mass of the 2α and $p + 2\alpha$ subevents. These very narrow states are the only intermediate resonances in the subevents that can be cleanly identified without significant underlying background. The excitation-energy spectra associated with the ≈100-keV-wide resonances, $^6\mathrm{Be}_{\mathrm{g.s.}}$ and the $5/2^-$ state in ^{9}B, could also be isolated with an indirect technique. Identification of states associated with even wider intermediate states was not possible. These techniques were also applied to the $3p + 2\alpha$ decay channel of ^{11}N for which previously unknown states were observed.

A number of democratic $2p$ emitters were identified in the ^{10}C and ^{11}N states associated with α-cluster structure. In particular, we have tentatively identified the first three members of the excited 0_2^+ band in ^{10}C with all observed members showing some probability for $2p$ emission. The large moment-of-inertia of this band is very similar to that for the analog structure in the mirror ^{10}Be and the 2^+ and 4^+ members, which are above the α threshold, also have large reduced widths for α decay. The spins of the first two members were deduced from comparison of the momentum correlations measured for their $2p$ branches to known 0^+ and 2^+ two-proton emitters of similar mass.

A second $3/2^-$ state was observed in ^{11}N which $2p$ decays to the ground state of ^{9}B. Possibly this state has a strong α-cluster structure which would be associated with a $K = 3/2^-$ rotational band. We have tentatively identified all members of this band up to $J = 9/2^-$. These members have very similar excitation energies to their counterparts in the mirror nucleus ^{11}Be proposed by Bohlen *et al.* [47].

Two more $2p$ emitters were observed in ^{11}N at $E^* =$ 9.271(58) and 11.047(67) MeV. Both of these states $2p$ decay to the lowest $5/2^-$ intermediate state of ^{9}B. The momentum correlations in these cases are also consistent with the results for $^{12}\mathrm{O}_{\mathrm{g.s.}}$ and $^{16}\mathrm{Ne}_{\mathrm{g.s.}}$, but the significance of this is not clear as the $2p$ decay energy of these two ^{11}N states are significantly larger than those for the ground-state emitters. Further work is needed to constrain the structure of these states.

ACKNOWLEDGMENTS

This material is based upon work supported by the U.S. Department of Energy, Office of Science, Office of Nuclear Physics under Award No. DE-FG02-87ER-40316. We thank S. Wang for fruitful discussions.

[1] O. Bochkarev, L. Chulkov, A. Korsheninniicov, E. Kuz'min, I. Mukha, and G. Yankov, Democratic decay of ^{6}Be states, Nucl. Phys. A **505**, 215 (1989).

[2] M. Pfützner, M. Karny, L. V. Grigorenko, and K. Riisager, Radioactive decays at limits of nuclear stability, Rev. Mod. Phys. **84**, 567 (2012).

[3] L. Grigorenko, T. Wiser, K. Miernik, R. Charity, M. Pfützner, A. Banu, C. Bingham, M. Ćwiok, I. Darby, W. Dominik, J. Elson, T. Ginter, R. Grzywacz, Z. Janas, M. Karny, A. Korgul, S. Liddick, K. Mercurio, M. Rajabali, K. Rykaczewski *et al.*, Complete correlation studies of two-proton decays: ^{6}Be and ^{45}Fe, Phys. Lett. B **677**, 30 (2009).

[4] S. M. Wang and W. Nazarewicz, Puzzling Two-Proton Decay of ^{67}Kr, Phys. Rev. Lett. **120**, 212502 (2018).

[5] S. M. Wang, W. Nazarewicz, R. J. Charity, and L. G. Sobotka, Structure and decay of the extremely proton-rich nuclei ^{11,12}O, Phys. Rev. C **99**, 054302 (2019).

[6] S. M. Wang, W. Nazarewicz, R. J. Charity, and L. G. Sobotka, Nucleon-nucleon correlations in the extreme oxygen isotopes, arXiv:2108.08007.

[7] I. A. Egorova, R. J. Charity, L. V. Grigorenko, Z. Chajecki, D. Coupland, J. M. Elson, T. K. Ghosh, M. E. Howard, H. Iwasaki, M. Kilburn, J. Lee, W. G. Lynch, J. Manfredi, S. T. Marley, A. Sanetullaev, R. Shane, D. V. Shetty, L. G. Sobotka, M. B.

Tsang, J. Winkelbauer *et al.*, Democratic Decay of ^{6}Be Exposed by Correlations, Phys. Rev. Lett. **109**, 202502 (2012).

[8] K. W. Brown, R. J. Charity, L. G. Sobotka, L. V. Grigorenko, T. A. Golubkova, S. Bedoor, W. W. Buhro, Z. Chajecki, J. M. Elson, W. G. Lynch, J. Manfredi, D. G. McNeel, W. Reviol, R. Shane, R. H. Showalter, M. B. Tsang, J. R. Winkelbauer, and A. H. Wuosmaa, Interplay between sequential and prompt two-proton decay from the first excited state of ^{16}Ne, Phys. Rev. C **92**, 034329 (2015).

[9] T. B. Webb, R. J. Charity, J. M. Elson, D. E. M. Hoff, C. D. Pruitt, L. G. Sobotka, K. W. Brown, J. Barney, G. Cerizza, J. Estee, G. Jhang, W. G. Lynch, J. Manfredi, P. Morfouace, C. Santamaria, S. Sweany, M. B. Tsang, T. Tsang, S. M. Wang, Y. Zhang *et al.*, Particle decays of levels in ^{11,12}N and ^{12}O investigated with the invariant-mass method, Phys. Rev. C **100**, 024306 (2019).

[10] M. F. Jager, R. J. Charity, J. M. Elson, J. Manfredi, M. H. Mahzoon, L. G. Sobotka, M. McCleskey, R. G. Pizzone, B. T. Roeder, A. Spiridon, E. Simmons, L. Trache, and M. Kurokawa, Two-proton decay of ^{12}O and its isobaric analog state in ^{12}N, Phys. Rev. C **86**, 011304(R) (2012).

[11] K. W. Brown, W. W. Buhro, R. J. Charity, J. M. Elson, W. Reviol, L. G. Sobotka, Z. Chajecki, W. G. Lynch, J. Manfredi, R. Shane, R. H. Showalter, M. B. Tsang, D. Weisshaar, J. R. Winkelbauer, S. Bedoor, and A. H. Wuosmaa, Two-proton decay from the isobaric analog state in ^{8}B, Phys. Rev. C **90**, 027304 (2014).

[12] R. J. Charity, J. M. Elson, J. Manfredi, R. Shane, L. G. Sobotka, Z. Chajecki, D. Coupland, H. Iwasaki, M. Kilburn, J. Lee, W. G. Lynch, A. Sanetullaev, M. B. Tsang, J. Winkelbauer, M. Youngs, S. T. Marley, D. V. Shetty, A. H. Wuosmaa, T. K. Ghosh, and M. E. Howard, $2p$-$2p$ decay of ^{8}C and isospin-allowed $2p$ decay of the isobaric-analog state in ^{8}B, Phys. Rev. C **82**, 041304(R) (2010).

[13] R. J. Charity, J. M. Elson, J. Manfredi, R. Shane, L. G. Sobotka, B. A. Brown, Z. Chajecki, D. Coupland, H. Iwasaki, M. Kilburn, J. Lee, W. G. Lynch, A. Sanetullaev, M. B. Tsang, J. Winkelbauer, M. Youngs, S. T. Marley, D. V. Shetty, A. H. Wuosmaa, T. K. Ghosh *et al.*, Investigations of three-, four-, and five-particle decay channels of levels in light nuclei created using a ^{9}C beam, Phys. Rev. C **84**, 014320 (2011).

[14] K. W. Brown, R. J. Charity, J. M. Elson, W. Reviol, L. G. Sobotka, W. W. Buhro, Z. Chajecki, W. G. Lynch, J. Manfredi, R. Shane, R. H. Showalter, M. B. Tsang, D. Weisshaar, J. R. Winkelbauer, S. Bedoor, and A. H. Wuosmaa, Proton-decaying states in light nuclei and the first observation of ^{17}Na, Phys. Rev. C **95**, 044326 (2017).

[15] R. J. Charity, T. D. Wiser, K. Mercurio, R. Shane, L. G. Sobotka, A. H. Wuosmaa, A. Banu, L. Trache, and R. E. Tribble, Continuum spectroscopy with a ^{10}C beam: Cluster structure and three-body decay, Phys. Rev. C **80**, 024306 (2009).

[16] R. B. Wiringa, S. C. Pieper, J. Carlson, and V. R. Pandharipande, Quantum Monte Carlo calculations of $A = 8$ nuclei, Phys. Rev. C **62**, 014001 (2000).

[17] W. von Oertzen, Dimers based on the $\alpha + \alpha$ potential and chain states of carbon isotopes, Z. Phys. A: Hadrons Nucl. **357**, 355 (1997).

[18] M. Freer, J. C. Angélique, L. Axelsson, B. Benoit, U. Bergmann, W. N. Catford, S. P. G. Chappell, N. M. Clarke, N. Curtis, A. D'Arrigo, E. de Goes Brennard, O. Dorvaux, B. R. Fulton, G. Giardina, C. Gregori, S. Grévy, F. Hanappe, G. Kelly, M. Labiche, C. Le Brun *et al.*, Exotic Molecular States in ^{12}Be, Phys. Rev. Lett. **82**, 1383 (1999).

[19] M. Freer, E. Casarejos, L. Achouri, C. Angulo, N. I. Ashwood, N. Curtis, P. Demaret, C. Harlin, B. Laurent, M. Milin, N. A. Orr, D. Price, R. Raabe, N. Soić, and V. A. Ziman, $\alpha : 2n : \alpha$ Molecular Band in ^{10}Be, Phys. Rev. Lett. **96**, 042501 (2006).

[20] M. Wallace, M. Famiano, M.-J. van Goethem, A. Rogers, W. Lynch, J. Clifford, F. Delaunay, J. Lee, S. Labostov, M. Mocko, L. Morris, A. Moroni, B. Nett, D. Oostdyk, R. Krishnasamy, M. Tsang, R. de Souza, S. Hudan, L. Sobotka, R. Charity *et al.*, The high resolution array (HiRA) for rare isotope beam experiments, Nucl. Instrum. Methods Phys. Res., Sect. A **583**, 302 (2007).

[21] K. Mercurio, R. J. Charity, R. Shane, L. G. Sobotka, J. M. Elson, M. Famiano, A. H. Wuosmaa, A. Banu, C. Fu, L. Trache, R. E. Tribble, and A. M. Mukhamedzhanov, Correlated two-proton decay from ^{10}C, Phys. Rev. C **78**, 031602(R) (2008).

[22] L. V. Grigorenko, T. D. Wiser, K. Mercurio, R. J. Charity, R. Shane, L. G. Sobotka, J. M. Elson, A. H. Wuosmaa, A. Banu, M. McCleskey, L. Trache, R. E. Tribble, and M. V. Zhukov, Three-body decay of ^{6}Be, Phys. Rev. C **80**, 034602 (2009).

[23] K. W. Brown, R. J. Charity, L. G. Sobotka, Z. Chajecki, L. V. Grigorenko, I. A. Egorova, Y. L. Parfenova, M. V. Zhukov, S. Bedoor, W. W. Buhro, J. M. Elson, W. G. Lynch, J. Manfredi, D. G. McNeel, W. Reviol, R. Shane, R. H. Showalter, M. B. Tsang, J. R. Winkelbauer, and A. H. Wuosmaa, Observation of Long-Range Three-Body Coulomb Effects in the Decay of ^{16}Ne, Phys. Rev. Lett. **113**, 232501 (2014).

[24] R. J. Charity, K. W. Brown, J. Elson, W. Reviol, L. G. Sobotka, W. W. Buhro, Z. Chajecki, W. G. Lynch, J. Manfredi, R. Shane, R. H. Showalter, M. B. Tsang, D. Weisshaar, J. Winkelbauer, S. Bedoor, D. G. McNeel, and A. H. Wuosmaa, Invariant-mass spectroscopy of ^{18}Ne, ^{16}O, and ^{10}C excited states formed in neutron-transfer reactions, Phys. Rev. C **99**, 044304 (2019).

[25] R. J. Charity, K. W. Brown, J. Okołowicz, M. Płoszajczak, J. M. Elson, W. Reviol, L. G. Sobotka, W. W. Buhro, Z. Chajecki, W. G. Lynch, J. Manfredi, R. Shane, R. H. Showalter, M. B. Tsang, D. Weisshaar, J. R. Winkelbauer, S. Bedoor, and A. H. Wuosmaa, Invariant-mass spectroscopy of ^{14}O excited states, Phys. Rev. C **100**, 064305 (2019).

[26] T. B. Webb, S. M. Wang, K. W. Brown, R. J. Charity, J. M. Elson, J. Barney, G. Cerizza, Z. Chajecki, J. Estee, D. E. M. Hoff, S. A. Kuvin, W. G. Lynch, J. Manfredi, D. McNeel, P. Morfouace, W. Nazarewicz, C. D. Pruitt, C. Santamaria, J. Smith, L. G. Sobotka *et al.*, First Observation of Unbound ^{11}O, the Mirror of the Halo Nucleus ^{11}Li, Phys. Rev. Lett. **122**, 122501 (2019).

[27] T. B. Webb, R. J. Charity, J. M. Elson, D. E. M. Hoff, C. D. Pruitt, L. G. Sobotka, K. W. Brown, J. Barney, G. Cerizza, J. Estee, W. G. Lynch, J. Manfredi, P. Morfouace, C. Santamaria, S. Sweany, M. B. Tsang, T. Tsang, Y. Zhang, K. Zhu, S. A. Kuvin *et al.*, Invariant-mass spectrum of ^{11}O, Phys. Rev. C **101**, 044317 (2020).

[28] R. J. Charity, L. G. Sobotka, and J. A. Tostevin, Single-nucleon knockout cross sections for reactions producing resonance states at or beyond the drip line, Phys. Rev. C **102**, 044614 (2020).

[29] R. J. Charity, T. B. Webb, J. M. Elson, D. E. M. Hoff, C. D. Pruitt, L. G. Sobotka, K. W. Brown, G. Cerizza, J. Estee, W. G. Lynch, J. Manfredi, P. Morfouace, C. Santamaria, S. Sweany,

C. Y. Tsang, M. B. Tsang, Y. Zhang, K. Zhu, S. A. Kuvin, D. McNeel *et al.*, Observation of the Exotic Isotope ^{13}F Located Four Neutrons Beyond the Proton Drip Line, Phys. Rev. Lett. **126**, 132501 (2021).

[30] Evaluated Nuclear Structure Data File (ENSDF), http://www.nndc.bnl.gov/ensdf/ (2021).

[31] A. M. Lane and R. G. Thomas, *R*-matrix theory of nuclear reactions, Rev. Mod. Phys. **30**, 257 (1958).

[32] T. Goigoux, P. Ascher, B. Blank, M. Gerbaux, J. Giovinazzo, S. Grévy, T. Kurtukian Nieto, C. Magron, P. Doornenbal, G. G. Kiss, S. Nishimura, P.-A. Söderström, V. H. Phong, J. Wu, D. S. Ahn, N. Fukuda, N. Inabe, T. Kubo, S. Kubono, H. Sakurai *et al.*, Two-Proton Radioactivity of ^{67}Kr, Phys. Rev. Lett. **117**, 162501 (2016).

[33] L. V. Grigorenko and M. V. Zhukov, Two-proton radioactivity and three-body decay. II. Exploratory studies of lifetimes and correlations, Phys. Rev. C **68**, 054005 (2003).

[34] K. Miernik, W. Dominik, Z. Janas, M. Pfützner, L. Grigorenko, C. R. Bingham, H. Czyrkowski, M. Ćwiok, I. G. Darby, R. Dabrowski, T. Ginter, R. Grzywacz, M. Karny, A. Korgul, W. Kuśmierz, S. N. Liddick, M. Rajabali, K. Rykaczewski, and A. Stolz, Two-Proton Correlations in the Decay of ^{45}Fe, Phys. Rev. Lett. **99**, 192501 (2007).

[35] S. M. Wang and W. Nazarewicz, Fermion Pair Dynamics in Open Quantum Systems, Phys. Rev. Lett. **126**, 142501 (2021).

[36] H. T. Fortune and R. Sherr, Structure of ^{16}Ne ground state, Phys. Rev. C **66**, 017301 (2002).

[37] L. V. Grigorenko, T. A. Golubkova, and M. V. Zhukov, Thomas-Ehrman effect in a three-body model: The ^{16}Ne case, Phys. Rev. C **91**, 024325 (2015).

[38] P. G. Sharov, L. V. Grigorenko, A. N. Ismailova, and M. V. Zhukov, Pauli-principle driven correlations in four-neutron nuclear decays, JETP Lett. **110**, 5 (2019).

[39] H. T. Fortune and R. Sherr, Constraints on energy of ^{9}B$(1/2^{+})$ and ^{10}C(0_2^{+}), Phys. Rev. C **73**, 064302 (2006).

[40] T. D. Baldwin, W. N. Catford, D. Mahboub, C. N. Timis, N. I. Ashwood, N. M. Clarke, N. Curtis, V. Ziman, T. A. D. Brown, S. P. Fox, B. R. Fulton, D. Groombridge, D. L. Watson, V. F. E. Pucknell, and D. C. Weisser, First excited $\frac{1}{2}^{+}$ state in ^{9}B, Phys. Rev. C **86**, 034330 (2012).

[41] H. Fortune, Narrow resonances in ^{11}N and ^{15}F, Nucl. Phys. A **968**, 342 (2017).

[42] K. T. Schmitt, K. L. Jones, A. Bey, S. H. Ahn, D. W. Bardayan, J. C. Blackmon, S. M. Brown, K. Y. Chae, K. A. Chipps, J. A. Cizewski, K. I. Hahn, J. J. Kolata, R. L. Kozub, J. F. Liang, C. Matei, M. Matoš, D. Matyas, B. Moazen, C. Nesaraja, F. M. Nunes *et al.*, Halo Nucleus ^{11}Be: A Spectroscopic Study Via Neutron Transfer, Phys. Rev. Lett. **108**, 192701 (2012).

[43] D. Morrissey, K. McDonald, D. Bazin, B. Brown, R. Harkewicz, N. Orr, B. Sherrill, G. Souliotis, M. Steiner, J. Winger, S. Yennello, B. Young, S. Lukyanov, G. Chubarian, and Y. Oganessian, Single neutron emission following ^{11}Li β-decay, Nucl. Phys. A **627**, 222 (1997).

[44] A. Bonaccorso, F. Cappuzzello, D. Carbone, M. Cavallaro, G. Hupin, P. Navrátil, and S. Quaglioni, Application of an *ab initio S* matrix to data analysis of transfer reactions to the continuum populating ^{11}Be, Phys. Rev. C **100**, 024617 (2019).

[45] N. Itagaki and S. Okabe, Molecular orbital structures in ^{10}Be, Phys. Rev. C **61**, 044306 (2000).

[46] M. Lyu, Z. Ren, B. Zhou, Y. Funaki, H. Horiuchi, G. Röpke, P. Schuck, A. Tohsaki, C. Xu, and T. Yamada, Investigation of ^{10}Be and its cluster dynamics with the nonlocalized clustering approach, Phys. Rev. C **93**, 054308 (2016).

[47] H. Bohlen, A. Blazevič, B. Gebauer, W. Von Oertzen, S. Thummerer, R. Kalpakchieva, S. Grimes, and T. Massey, Spectroscopy of exotic nuclei with multi-nucleon transfer reactions, Prog. Part. Nucl. Phys. **42**, 17 (1999).

[48] H. G. Bohlen, W. von Oertzen, R. Kalpakchieva, B. Gebauer, S. M. Grimes, A. Lenz, T. N. Massey, M. Milin, C. Schulz, T. Kokalova, S. Torilov, and S. Thummerer, Structure of neutron-rich Be and C isotopes, Phys. At. Nucl. **66**, 1494 (2003).

[49] S. Hamada, M. Yasue, S. Kubono, M. H. Tanaka, and R. J. Peterson, Cluster structures in ^{10}Be from the ^{7}Li$(\alpha, p)^{10}$ Be reaction, Phys. Rev. C **49**, 3192 (1994).

[50] M. Milin, M. Zadro, S. Cherubini, T. Davinson, A. Di Pietro, P. Figuera, D. Miljanić, A. Musumarra, A. Ninane, A. Ostrowski, M. Pellegriti, A. Shotter, N. Soić, and C. Spitaleri, Sequential decay reactions induced by a 18 MeV ^{6}He beam on ^{6}Li and ^{7}Li, Nucl. Phys. A **753**, 263 (2005).

[51] D. Brink, Kinematical effects in heavy-ion reactions, Phys. Lett. B **40**, 37 (1972).

[52] J. A. Liendo, N. Curtis, D. D. Caussyn, N. R. Fletcher, and T. Kurtukian-Nieto, Near threshold three-body final states in ^{7}Li + ^{7}Li reactions at $E_{\rm lab} = 34$MeV, Phys. Rev. C **65**, 034317 (2002).

[53] T. Teichmann and E. P. Wigner, Sum rules in the dispersion theory of nuclear reactions, Phys. Rev. **87**, 123 (1952).

[54] M. J. Schneider, B. W. Ridley, M. E. Rickey, J. J. Kraushaar, and W. R. Zimmerman, Study of unbound levels in ^{10}C via ^{10}B(^{3}He, t), Phys. Rev. C **12**, 335 (1975).

[55] P. Descouvemont, Microscopic study of α clustering in the ^{9,10,11}Be isotopes, Nucl. Phys. A **699**, 463 (2002).

[56] R. J. Charity, S. A. Komarov, L. G. Sobotka, J. Clifford, D. Bazin, A. Gade, Jenny Lee, S. M. Lukyanov, W. G. Lynch, M. Mocko, S. P. Lobastov, A. M. Rogers, A. Sanetullaev, M. B. Tsang, M. S. Wallace, S. Hudan, C. Metelko, M. A. Famiano, A. H. Wuosmaa, and M. J. van Goethem, Particle decay of ^{12}Be excited states, Phys. Rev. C **76**, 064313 (2007).

[57] A. Saito, A. Shimoura, Y. U. Matsuyama, H. Baba, N. Aoi, T. Gomi, Y. Higurashi, K. Ieki, N. I. N. Imai, S. Hanno, S. Kubono, M. Kunibu, S. Michimasa, T. Motobayashi, T. Nakamura, H. Ryuto, H. Sakurai, M. Serata, E. Takeshita, S. Takeuchi *et al.*, The ^{6}He + ^{6}He and α + ^{8}He cluster states in ^{12}Be via α-inelastic scattering, Mod. Phys. Lett. A **25**, 1858 (2010).